Autonomous profiling float observations of the high biomass plume downstream of the Kerguelen plateau in the Southern Ocean

M. Grenier[1*], A. Della Penna[2], and T. W. Trull[3]

1. Antarctic Climate and Ecosystems Cooperative Research Centre, Hobart, Tasmania, Australia, and Laboratoire d'Etudes en Géophysique et Océanographie Spatiales (CNRS/CNES/IRD/University of Toulouse), Toulouse, France. Now at Earth, Ocean and Atmospheric Sciences (University of British Columbia), Vancouver, Canada.
2. Quantitative Marine Sciences PhD Program, Institute for Marine and Antarctic Studies, University of Tasmania, and Commonwealth Scientific and Industrial Research Organisation, Hobart, Tasmania, Australia, and Sorbonne Universités, UPMC Univ Paris 06, UMR 7159, LOCEAN-IPSL, F-75005, Paris, France and Univ Paris Diderot Cité
3. Commonwealth Scientific and Industrial Research Organisation, Oceans and Atmosphere Flagship, Hobart, Tasmania, Australia, and Antarctic Climate and Ecosystems Cooperative Research Centre, Hobart, Tasmania, Australia

*Corresponding author: melaniegrenier14@yahoo.fr

Abstract

Natural iron fertilisation from Southern Ocean islands results in high primary production and phytoplankton biomass accumulations readily visible in satellite ocean colour observations. These images reveal great spatial complexity with highly varying concentrations of chlorophyll, presumably reflecting both variations in iron supply and conditions favouring phytoplankton accumulation. To examine the second aspect, in particular the influences of variations in temperature and mixed layer depth, we deployed four autonomous profiling floats in the Antarctic Circumpolar Current near the Kerguelen plateau in the Indian sector of the Southern Ocean. Each 'bio-profiler' measured more than 250 profiles of temperature (T), salinity (S), dissolved oxygen, chlorophyll-a (Chl-a) fluorescence, and particulate backscattering (b_{bp}) in the top 300 meters of the water column, sampling up to 5 profiles per day along meandering trajectories extending up to 1000 km. Comparison of surface Chl-a estimates (analogous to values from satellite images) with total water column inventories revealed largely linear relationships, suggesting that these images provide credible information on total and not just surface biomass accumulations. Regions of very high Chl-a accumulation (1.5-10 $\mu g\ L^{-1}$) were associated predominantly with a narrow T-S class of surface waters. In contrast, waters with only moderate Chl-a enrichments (0.5-1.5 $\mu g\ L^{-1}$) displayed no clear correlation with specific water properties, including no dependence on mixed layer depth or the intensity of stratification. Geostrophic trajectory analysis suggests that both these observations can be explained if the main determinant of biomass in a given water parcel is the time since leaving the Kerguelen plateau. One float became trapped in a cyclonic eddy, allowing temporal evaluation of the water column in early autumn. During this period, decreasing surface Chl-a inventories corresponded with decreases in oxygen inventories on sub-mixed layer density surfaces, consistent with significant export of organic matter (~35%) and its respiration and storage as dissolved inorganic carbon in the ocean interior. These results are encouraging for the expanded use of autonomous observing platforms to study biogeochemical, carbon cycle, and ecological problems, although the complex blend of Lagrangian and Eulerian sampling achieved by the floats suggests that arrays rather than single floats will often

46 be required, and that frequent profiling offers important benefits in terms of resolving the role of
47 mesoscale structures on biomass accumulation.

1 Introduction

The productivity of the Southern Ocean is important for many reasons. It supports fisheries and high conservation value marine mammal and bird populations (Constable et al., 2003; Nicol et al., 2000), influences the carbon dioxide content of the atmosphere (Sarmiento and Le Quéré, 1996; Sigman and Boyle, 2000; Watson et al., 2000), and affects the magnitude of nutrient supply to large portions of the global surface ocean (Sarmiento et al., 2004). This productivity is limited by the scarce availability of iron (Fe) as an essential micro-nutrient (Boyd and Ellwood, 2010; Boyd et al., 2007; Martin, 1990). Island sources of Fe elevate productivity and produce downstream 'plumes' of elevated phytoplankton biomass that contrasts with the general HNLC (High Nutrients, Low Chlorophyll) nature of the Southern Ocean (Blain et al., 2007; de Baar et al., 1995; Mongin et al., 2009; Pollard et al., 2009; Nielsdóttir et al., 2012). Ship based studies of several of these regions, focused on the influence of Fe on carbon (C) transfer to the ocean interior (Blain et al., 2008; Salter et al., 2007), have revealed a diversity of responses in terms of intensity of enhanced productivity, biomass accumulation, and ecosystem structures. This diversity derives from interactions between the supply and bio-availability of iron with other drivers of productivity such as temperature, water column stratification and stability, light levels, and the possibility of co-limitation by other nutrients (Assmy et al., 2013; Boyd et al., 1999, 2001; Queguiner, 2013).

Assessing influences on productivity, biomass accumulation, carbon export, and carbon dioxide (CO_2) uptake in the Southern Ocean is challenging because of variations across many scales, including weather, seasonal, and interannual time-scales, and sub-mesoscale, mesoscale, and circumpolar frontal space scales (Joubert et al., 2014; Le Quéré et al., 2010; Lenton et al., 2013; Levy, 2003; Nicol et al., 2000; Shadwick et al., 2015; Sokolov and Rintoul, 2007; Swart et al., 2014; Thomalla et al., 2011; Weeding and Trull, 2014). Satellite observations offer extensive space-time coverage (Martinez et al., 2009; Moore and Abbott, 2000), but may provide a biased view if surface distributions are not representative of water column inventories. Important ways that bias could arise include lack of direct correlations of surface values with their vertical extents (e.g. high surface

chlorophyll values might be predominantly associated with shallow accumulations, through the promotion of production by higher light levels in shallow mixed layers; Sverdrup, 1953), the presence of unobserved subsurface chlorophyll maxima (Carranza et al., 2014; Schlitzer, 2002), or the variation of phytoplankton to chlorophyll ratios with growth conditions (Cloern et al., 1995; Fennel and Boss, 2003; Goericke and Montoya, 1998).

These difficulties of observation become even more acute for carbon export estimates, which require either flux measurements (e.g. from moored or free-drifting sediment traps or radionuclide activities (Planchon et al., 2014; Savoye et al., 2008) or the partitioning of changes in state variables across biogeochemical versus oceanographic causes (e.g. nitrate depletions in surface waters or oxygen consumption at mesopelagic depth; Matear et al., 2000; Trull et al., 2015). Obtaining estimates of carbon export and the depth of its penetration into the ocean interior are important to determining impacts on the climate system, because variations in these two factors have similar influence to variations in total primary production in terms of the sequestration of CO_2 from the atmosphere (Boyd and Trull, 2007). Notably, export estimates expressed as 'e-ratio' fractions of primary production (Maiti et al., 2013), or as 'f-ratio' fractions of production derived from 'new' nitrate supply (Savoye et al., 2004) vary widely in the Southern Ocean, with the possibility that these efficiencies are increased by natural iron fertilisation (Jouandet et al., 2011; Trull et al., 2008).

This space-time complexity is abundantly demonstrated by the 'mosaic of blooms' (i.e. patchiness pattern) encountered in waters downstream from the Kerguelen plateau during the KEOPS2 field program in austral spring (October-November 2011), as detailed in many papers in a special volume of Biogeosciences (d'Ovidio et al., 2014; Trull et al., 2015; Lasbleiz et al., 2014; Laurenceau-Cornec et al., 2015; Cavagna et al., 2014). Much of the meso-scale spatial variations in biomass accumulation, as seen in satellite images and animations (Mongin et al., 2009; d'Ovidio et al., 2014; Trull et al., 2015), appears to result from the interleaving of iron-enriched water parcels that have transited the Kerguelen plateau with surrounding iron poor waters, as demonstrated by analysis of satellite

altimetry based circulation estimates and surface drifter trajectories (Park et al., 2014a; d'Ovidio et al., 2014). However, shipboard studies close to the plateau (Mosseri et al., 2008; d'Ovidio et al., 2014; Blain et al., 2015; Trull et al., 2015; Lasbleiz et al., 2014; Laurenceau-Cornec et al., 2015) suggest that other factors are also likely to play a role, including mixed layer depth and upper water column stratification.

To explore the influence of variations in these water column properties on bloom structure at larger scale, in particular further from the plateau than could be surveyed by ship, we deployed autonomous profiling drifters. The first one was successfully launched during the KEOPS2 field program in late October 2011, and the other three during the MyctO-3D-MAP (referred to as MYCTO, from now on in this text) interdisciplinary survey between late January and early February 2014. Given the extent of the Kerguelen biomass plume (> 1000 km; Mongin et al., 2009), the remoteness from ports, and the generally rough sea states, the use of autonomous platforms is arguably the only affordable way to survey this region. As shown in Figure 1, these deployments returned data from a large proportion of the enriched biomass plume downstream of the Kerguelen plateau.

In this paper, we use the bio-profiler observations to address three questions:

1) Do satellite images of surface chlorophyll provide an unbiased guide to the spatial distribution of total water column chlorophyll, or are they biased by lack of knowledge of variations in the vertical extent of chlorophyll distributions or the presence of subsurface chlorophyll maxima?

2) Do regions of high biomass correlate with particular oceanographic properties, such as warmer or fresher waters, or the intensity of stratification? If so, are these properties determined locally or by the upstream origins of the different water parcels?

3) Can the fate of surface enrichments in biomass be determined (and eventually quantified) from along-trajectory temporal variations in biogeochemical properties, for example by progressive

downward movement of fluorescence or particulate backscattering signals or decreases of oxygen in subsurface waters?

2 Methods

2.1 Float sensor and mission configurations

The float deployment locations are provided in Table 1, along with their identification numbers which provide access to their full data sets via the Australian Integrated Marine Observing System (www.imos.org.au). Float deployment was done in 2011 by manual transfer to a small boat and then the sea, and in 2014 by deploying the floats from the ship deck inside cardboard boxes designed to readily disintegrate after release. The autonomous profiling floats were all of the same design (Model APF9I, Teledyne-Webb, Inc.). Each was equipped with pumped, poisoned, thermosalinographs (Model SBE 41CP-2.0, Seabird, Inc.), end-cap mounted un-pumped oxygen optodes (Model 3830, Aanderaa, Inc.), and two-channel bio-optical sensors (Model FLBBAP2, Wetlabs, Inc.) strapped onto the lower third of the float hull with their optical ports facing horizontally to minimize possible interferences from particle accumulation. Owing to the structure of the firmware for the floats and the varying power requirements for the sensors, the sampling rates differed for the physical and biogeochemical parameters. Temperature and salinity were sampled at the highest rates, yielding values at 2 decibar intervals (used in this work as equivalent to 2 meter depth intervals without density corrections), whereas oxygen, fluorescence and backscatter were sampled at 10 decibar intervals, except for bio-profiler #1 where they were sampled at 5 decibar intervals in the first 150 m.

Temperature and salinity calibrations were performed by Seabird, Inc., with estimated accuracy and precision of better than 0.005 °C and 0.01, respectively (Oka and Ando, 2004). These variables, used as water mass proxies and to estimate mixed layer depths and stratification intensity (expressed as the Brunt-Väisälä frequency), helped to determine if dissolved oxygen evolutions were mainly due

147 to physical processes or to biological production or respiration processes. The oxygen optodes were
148 calibrated at CSIRO prior to mounting on the floats against a 20 point matrix of 4 temperatures (0.5
149 - 30) and 5 oxygen saturations (0 - 129%) using the methods detailed in Weeding and Trull (2014).
150 Similar sensors exhibited drift during a 6 month mooring deployment in the Southern Ocean of less
151 than 1.7 µmol kg^{-1} over 6 months (Weeding and Trull, 2014).

152 The bio-optical sensors measured chlorophyll-a fluorescence via stimulation/emission at 470/695
153 nm) and particulate backscattering at 700 nm. Chlorophyll-a fluorescence is a useful proxy for
154 chlorophyll-a concentration and standing stocks of phytoplankton biomass (Falkowski and Kiefer,
155 1985; Huot et al., 2007). Particulate backscattering provides a good proxy for particulate organic
156 carbon (Stramski et al. 2008; Cetinić et al, 2013). The bio-optical fluorescence sensors were calibrated
157 (by the manufacturer, Wetlabs, Inc.) against fluorescent uranine solutions as working standards, and
158 cross- referenced to prior measurements of a laboratory culture (25 mg m^{-3} chlorophyll) of the diatom
159 *Thallassiosira weissflogii* to yield chlorophyll estimates. These calibrations are warranted to yield
160 linear responses with precisions among multiple sensors of better than 10%, and (after one cycle of
161 testing and replacement with the manufacturer) we obtained reproducibility for the set of three floats
162 deployed in 2014 of better than 4% based on measurements with fluorescent and non-reflective
163 plastics (Earp et al., 2011). Accordingly, calculation of the chlorophyll fluorescence from the float
164 data was done by removal of the background dark signals measured prior to deployment and scaling
165 to chlorophyll using the manufacturer's calibrations. Similarly, the retrieval of particulate
166 backscattering, b_{bp} (m^{-1}), at 700 nm from the backscatter raw transmitted measurement (counts) was
167 done by applying the manufacturer-provided scaling factor after correction for dark counts (i.e.
168 measured signal output of the backscatterometer in clean water with black tape over the detector),
169 with the additional steps of removal of the pure seawater backscattering contribution (Zhang et al.,
170 2009), and scaling from the limited solid angle sensor measurement to the total backscattered
171 hemisphere based on relations estimated from observations for a wide range of marine particles (Boss
172 and Pegau, 2001; Sullivan et al., 2012).

In contrast to typical Argo program float missions for climate studies (www.argo.org), which consist of deep (2000 m) profiles every 10 days, the bio-profilers were programmed to focus on the upper water column and carried out continuous profiling between the surface and 300 m depth, achieving 4 to 6 profiles per day, depending on the stratification. This temporal resolution was intended to allow examination of daily cycles related to insolation, photosynthesis, and respiration. In practice, it proved difficult to extract clear cycles because of aliasing from spatial variations. Consequently, after several weeks for the 2011 KEOPS2 deployment of bio-profiler #1, the frequency of profiles was reduced to twice daily, to provide extended battery life while still obtaining night and day observations to allow insolation quenching of the fluorescence response to be evaluated and corrected, and thus to avoid inappropriate inference of subsurface chlorophyll maxima from the fluorescence signal (Sackmann et al., 2008; Xing et al., 2012). For bio-profilers #2, #3, and #4 deployed in 2014, the missions were further refined, via automated telemetric switching of mission configuration files, to carry out a deep profile to ~1500 m every 3 days to provide deep reference points for temperature, salinity, and oxygen observations, and also with the intention to slow the development of bio-fouling of the bio-optical sensors by exposing surface organisms to high pressures.

2.2 Float data quality control

Extensive experience by the Argo program with profiling float measurements for temperature (T) and salinity (S), including recovery of floats for post deployment tests (Oka and Ando, 1994), suggests that these sensors reliably deliver accurate and precise observations (to better than 0.005 °C and 0.01 salinity) over multi-annual deployments. Given our much shorter bio-profiler deployments (3 to 6 months) and their observed T-S relationships which fall within those of the ship-based KEOPS2 observations, we assume these variables are correct and make no further assessment or

197 correction. We similarly accept the oxygen observations, given our careful attention to their pre-
198 deployment calibration, their reasonable range of surface water oxygen super-saturations (96-103%
199 for low chlorophyll waters and extending up to 108% in correlation with very high chlorophyll waters,
200 as discussed further below), and their deep ocean values (950-1000 m depths) which fall within the
201 range of nearby ship observations and showed no temporal trends and standard deviations of less than
202 4 μmol kg^{-1} over the deployment periods (ranging from 1 to 3.9 μmol kg^{-1} for the four bio-profilers).

203 To evaluate the possibility of temporal sensor drifts in bio-optical variables, we examined the
204 variations of the bio-optical variables in mesopelagic (250-300 m) and deep water (950-1000 m)
205 values, i.e. at depths where little signal was anticipated and most profiles reached steady background
206 values (Figure 2a). The particulate backscattering and, to a lesser extent, the Chl-a fluorescence
207 signals showed spikes which presumably reflect larger particles such as aggregates and zooplankton,
208 motivating our examination of average values over 50 m ranges (250-300 m and 950-1000 m depth
209 layers) for the assessment of temporal drifts. As shown in Figure 2a and quantified in Table 2, for
210 most of their deployment periods all four bio-profilers exhibited no significant temporal drift of these
211 deep values except for bio-profiler #1, for which high and erratic values of Chl-a and b_{bp} began to
212 occur after profile #300 both at depth (Figure 2a) and throughout the water column (Figure 3.1c and
213 e). We consider this to be caused by bio-fouling and do not use this data in any subsequent analysis
214 (this loss of signal fidelity was one of the motivations for including periodic deep profiles in the
215 subsequent three bio-profiler deployments, as a means of retarding fouling). In contrast, the high
216 fluorescence chlorophyll values found in mesopelagic waters from profiles ~#100 to ~#170 along the
217 bio-profiler #1 trajectory appear to be real and to reflect the deep extension of high biomass
218 occurrence at this time, as discussed further below (see also Figure 3.1c). Consequently, this range of
219 profile was not taken into account for the drift calculation in Table 2. Overall, except for the bio-
220 profiler #1, most of the bio-optical sensors showed a slight loss of sensitivity with time, as indicated
221 by the negative slopes of the trend of their responses in the two considered depth layers (Table 2).
222 Over the time course of the bio-optical sensor observations, these sensor drifts were small in

223 comparison to the changes observed for surface bio-optical values, contributing less than 7% to either
224 fluorescence or particulate backscattering. The only exception was the drift for the bio-profiler #2 b_{bp}
225 sensor in the 250-300 m layer, where drift appeared to have been larger (though of course changes at
226 this depth range may also be oceanic) and reached up to 19 % of the low surface b_{bp} values for this
227 bio-profiler.

228 Fluorescence signals were also corrected for daytime quenching. This effect, which derives from
229 the photo-inhibition of phytoplankton by an excess of light (maximum at midday), decreases surface
230 fluorescence (Falkowski and Kolber, 1995; Kiefer, 1973) and, if uncorrected, can produce a false
231 impression of subsurface maxima in fluorescence derived chlorophyll profiles. We explain this
232 correction and its evaluation in considerable detail in the following paragraphs, but note that none of
233 the conclusions of the paper depend on these corrections because the same overall results are obtained
234 if we use only Chl-a fluorescence signals collected at night. Our purpose in detailing the correction
235 is to contribute to active discussion of the best way to use daylight Chl-a fluorescence data obtained
236 from platforms which may not have as good night time coverage as our floats (such as sensors
237 deployed on seals, on standard ARGO 10- day profile interval missions, or on float missions that
238 target co-measurement with daytime satellite ocean colour observations).

239 We defined the daytime profiles, potentially affected by quenching, as profiles acquired between
240 one hour after local sunrise time and one hour after local sunset time, to allow for dark acclimation
241 since quenching effect could still persist after sunset (Sackmann et al., 2008). Daytime profiles from
242 the four bio-profilers are shown to illustrate this effect (continuous lines in Figure 2b, left panel). To
243 correct this bias, we applied the method of Sackmann et al. (2008), which uses the particulate
244 backscattering signal as a relative reference. For the sake of consistency with the other studies of this
245 issue, we defined the mixed layer depth, MLD, as the depth where density increased by 0.02 kg m^{-3}
246 relative to the density at 10 m (Park et al., 1998). Within the deeper half of the mixed layer (targeted
247 to be below the depth of daytime quenching), we determined a mean value of the (relatively constant,

see below) Chl-a fluorescence to b_{bp} ratio (at depth defined as $d_{F/bbp}$) and multiplied this ratio by the b_{bp} signal at this depth to retrieve the Chl-a fluorescence. Then, we multiplied this same ratio by the surface b_{bp} value to estimate unquenched surface Chl-a fluorescence, and interpolated between these two depths to obtain the unquenched Chl-a fluorescence profile. This assumes that phytoplankton populations were not stratified within the density defined mixed layer. This works particularly well for deep mixed layers (>50 m) which exhibit relatively constant Chl-a fluorescence/b_{bp} ratios (to within ~10%) in their deeper half. In less than 3% of the daytime profiles, in average, we could not identify a region of uniform Chl-a fluorescence/b_{bp} and apply the quenching correction; consequently, these profiles were not used further.

The greater spikiness of the b_{bp} profiles in comparison to those of fluorescence (as illustrated in Figure 2b, right panels) means that this quenching correction introduces some noise into the daytime chlorophyll estimates. In principle, this could be filtered or smoothed, but the low 10 m vertical resolution of the observations made this rather uncertain and so we have used the unfiltered observations throughout this paper (except in Figure 9f below where we show median-filtered particulate backscattering profiles for the sake of visual clarity). Note that to avoid to correct the surface Chl-a fluorescence with a spiked surface b_{bp} value and create a "b_{bp} spiked" interpolation, we verified before that the b_{bp} surface value did not seem to be spiked, assuming that surface value should not exceed more than ±50% of the b_{bp} value at the depth $d_{F/bbp,}$ since within the mixed layer. This threshold was defined after assessing the backscatterometer precision (using the coefficient of variation of b_{bp}, i.e. the ratio of the standard deviation to the mean) between 500 and 1000 m depth of 14 ± 4% in average. If the surface b_{bp} value was considered as spiked (less than 4% of the daytime b_{bp} profiles, except for bio-profiler #4 for which it reached 9%), the test was done with the second depth value, until a "non-spiked" value was found, and the value was then extrapolated to the surface.

The effects of the quenching correction on our selected chlorophyll profiles are shown in Figure 2b (middle panels, continuous lines), and summary statistics for all the profiles are provided in Table 3. Without the correction, on average, more than 70% of the daytime profiles exhibited a subsurface

maximum exceeding 60% of the surface value –defined after assessing the fluorometer error (coefficient of variation of Chl-a concentration) between 250 and 300 m depth and between 500 and 1000 m depth of 22 ± 10% in average. After applying the quenching correction method, the number of daytime profiles exhibiting a subsurface maximum exceeding 60% of the surface value was reduced to very similar levels to those observed in the night time profiles, although slightly higher (of 21% in average), indicating, with the fact that these daytime subsurface maxima occurred mostly below the MLD, that the correction was largely successful. Notably, for the total data set, after quenching correction, less than 11% of the profiles exhibited a deep maximum exceeding 100% of the surface value (Table 3), and these profiles were primarily located in a restricted region near the Gallieni Spur, as discussed further in the Results section.

Even after our quenching correction, 10% of the corrected daytime profiles (in average for all 4 bio-profilers) still exhibited significant decrease of the Chl-a fluorescence in the surface layer. We were not able to conclude if these decreases were due to an incomplete quenching correction or if they were true features, given that ~ 14% of the night profiles in average exhibited subsurface values at least 60% higher than the surface values. Consequently, we defined a threshold surface value for each bio-profiler, defined as a slightly lower value than the minimum surface value reached during night profiles (see squares in Figure 2b, middle panel, and caption) and we flagged all the corrected daytime profiles that had a surface value lower than this threshold as potentially arising from incomplete correction of quenching. These distinctions between night, daytime and flagged profiles are illustrated in Figures 4, 5 and 7, and further discussed in the Results and Discussion sections below. Note that, using a different quenching correction method, Biermann et al. (2015) recently observed similar features and statistics in fluorescence profiles collected by southern elephant seals during austral summer in the vicinity of Kerguelen Island.

Finally, we emphasize that the bio-optical measures of chlorophyll and particulate backscattering are based on laboratory calibrations that are not specific to Southern Ocean phytoplankton or particle

properties. This means that while interpretation of local variations is reasonably straightforward, quantitative comparisons to other observations much more uncertain (except perhaps in the future for other serial numbers of these sensors, calibrated in the same limited way). For the 3 bio-profilers deployed in 2014, no ancillary shipboard measurements are available to evaluate this issue, but in 2011 some chlorophyll samples were collected by the KEOPS2 science team that allow for limited evaluation of the bio-profiler #1 calibration.

Bioprofiler #1 was deployed into a semi-permanent meander of the Polar Front, which the KEOP2 program examined as a Lagrangian time series following surface drifters. As shown in Figure 2c, the first and second stations in the meander (E1 CTD-27 on 29 October 2011 at 22:46 local time and E2 CTD-43 on 1 November 2011 at 12:00 local time) bracketed the locations of the first 11 autonomous bio-profiler #1 profiles (Figure 2c.i). The bio-profiler #1 temperature profiles are intermediate between the ship results (Figure 2c.ii), with the variations in temperature profiles mainly driven by vertical motions associated with internal waves (Park et al., 2014b). In Figure 2c.iii, the KEOPS2 shipboard fluorescence results are displayed after linear calibration to high pressure liquid chromatography (HPLC) total chlorophyll-a results from below 40 meters depth (below the depth of non-photochemical quenching). The data reveal two important features: i) good fits achieved below 40 meters do not extend to the surface – where fluorescence/chlorophyll-a ratios were higher than at depth, apparently as a result of community composition variations with depth (see also Lasbleiz et al. 2014), and ii) the bio-profiler #1 fluorescence data displayed similar characteristics and good accord with the shipboard results. In light of the limited available data, a non-linear calibration of fluorescence to chlorophyll-a was not pursued, and no adjustments were made to the laboratory bio-profiler calibration.

These variations in fluorescence/chlorophyll-a ratios within individual CTD casts in the shipboard observations serve as a strong reminder that fluorescence is an imperfect proxy for chlorophyll-a concentrations, owing to variations with phytoplankton community structure, physiology, and other effects (e.g. Babin et al., 1996; Cullen, 1982; Suggett et al., 2011). Thus,

interpretation of our sensor records, as with any bio-optical sensor results, must keep this in mind and avoid over-interpreting small variations in fluorescence as necessarily resulting from variations in chlorophyll or phytoplankton biomass.

2.3 Satellite data sources

We used satellite products to provide physical and biological context for the bio-profiler trajectories, including the effectiveness of their sampling of high biomass waters downstream of Kerguelen. The images of surface chlorophyll concentrations shown in Figure 1 to provide context for the plume sampling achieved by the bio-profilers are the CLS SSALTO/DUACS 4 km daily product derived from NASA MODIS-Aqua observations (Figure 1), without modification for recent suggestions that this algorithm may underestimate chlorophyll in low chlorophyll waters south of Australia (Johnson et al., 2013).

To better understand the observed bio-profiler trajectories, we calculated expected movements based on geostrophic currents estimated from satellite altimetry using the multi-satellite global product Delayed Time Maps of Absolute Dynamic Heights (DT-MADT) developed by the CNES/CLS Aviso project (www.aviso.oceanobs.com). This product has 1 week temporal and 1/3° spatial resolutions, and was used to compute Lagrangian trajectories to produce a diagnostic for eddy retention (d'Ovidio et al., 2013; Figure 9b) and water origin and age (d'Ovidio et al., 2014; Figure 8). Eddy retention is a measure of how much time a synthetic water parcel has been recirculating within an eddy core. Long-lived and coherent eddies are characterised by water parcels with high values of retention (measured in days since a water parcel has been entrained by an eddy), whereas recently formed eddies or eddies that exchange strongly with surrounding regions have low retention values. Following d'Ovidio et al. (2014) and Sanial et al. (2014), we used back-tracking of virtual water parcels (from the bio-profiler profile locations) to compute how long ago (water age) and at which latitude (water origin) the sampled parcels had been in contact with the Kerguelen Plateau (defined

as the 700 m isobath, as shown in red in Figure 3.1). Figure 8 a) and c), adapted from d'Ovidio et al. (2014), display example maps of the calculated daily snapshots of these water ages and water origins. For each pixel in these maps, virtual water parcels were back tracked for 90 days. They are shown as white pixels on the maps if during that time they never touched the Kerguelen Plateau (shown in grey on the map), and otherwise are coloured for the time between the contact with the plateau and the day of the map computation (water age, Figure 8a) and the latitude of the last contact with the plateau stored (water origin, Figure 8c). These same computations were performed for each location sampled by the bio-profilers, in order to compare the water ages and origins with their measured chlorophyll inventories.

3 Results

3.1 Coverage of the plume

The drifts of the bio-profilers provided coverage of a large portion of the elevated biomass plume (Figure 1), from near the Kerguelen plateau to more than 700 miles downstream (71 to 95° E) and nearly 400 miles from north to south (47.5 to 54° S), thereby spanning waters of the Polar Frontal and Antarctic Zones (Orsi et al., 1995; Park et al., 2008b; Sokolov and Rintoul, 2009). Unfortunately, this breadth of spatial coverage of the plume did not extend to full temporal seasonal coverage, and this is important to keep in mind given the strong seasonal cycle of biomass accumulation (Trull et al., 2015; Blain et al., 2007; Mongin et al., 2008). As shown in these images, the 2011 bio-profiler covered the period of highest biomass accumulation, while the 2014 deployments occurred after this seasonal peak, and thus sampled the system during its senescence (to illustrate these prior conditions, Figure 1 also includes biomass distribution images from late 2013, before the launch of the three bio-profilers in early 2014). Thus, the profilers obtained some seasonal context for the central portion of the plume (which was sampled well in 2011 by bio-profiler #1 in spring and summer and again by bio-profilers #2 and #3 in summer and autumn). However, sampling of the north-eastern portion of

374 the downstream plume (north of the Polar Front) was achieved only in late summer and autumn (by
375 bio-profiler #4).

376 Bio-profiler #1 in spring 2011 and bio-profiler #3 in 2014 were deployed in the centre of the
377 quasi-stationary cyclonic recirculation just east of the northern Kerguelen plateau (d'Ovidio et al.,
378 2014; Park et al., 2014a). Both bio-profilers exited this region to the northeast, tracking towards the
379 Gallieni Spur, before transiting strongly southward near 74° E. This southward transport has also
380 been observed for surface drifters and appears to be associated with a persistent meander of the Polar
381 Front (d'Ovidio et al., 2014; Park et al., 2014a). Thus bio-profilers #1 and #3 provide spring and
382 summer perspectives respectively for these portions of the biomass plume (albeit in different years).

383 Bio-profiler #2 was deployed further south, close to the region where the strong north to south
384 transport portions of the bio-profilers #1 and #3 trajectories finished. Thus bio-profiler #2 provided
385 some overlap with the southern portion of the bio-profiler #1 trajectory, before being carried the
386 furthest south, where it explored cold waters close to the Williams Ridge that extends to the southeast
387 of Heard Island and terminates near the Fawn Trough (a gap in the plateau which permits the passage
388 of much of the deep water eastward transport; Park et al., 2008b; 2014a). Waters in this region tend
389 to exhibit archetypical high-nutrient, low-chlorophyll characteristics, and were used as a reference
390 station for iron non-fertilised waters during the KEOPS field program in 2005 (Blain et al., 2007;
391 2008).

392 In contrast, bio-profiler #4 was deployed at similar latitude to bio-profilers #1 and #3, but further
393 east, in particular east of the southward meander of the Polar Front which carried these others to the
394 south. Bio-profiler #4 remained in the northern portion of the plume throughout its deployment,
395 drifting to the northeast roughly parallel to the shallow Eastern Kerguelen Ridge before becoming
396 trapped in a cyclonic eddy in which it obtained a time series of ~100 profiles (as discussed in detail
397 below).

398

399 **3.2 Overview of observed oceanographic properties**

400 The bio-profilers return a large number of water column observations making visualisation at the
401 scale of individual profiles only possible for targeted issues. The simplest first-order assessment is
402 most easily done by presenting the results as along-trajectory sections. These are shown for all the
403 observed variables for each bio-profiler in Figures 3.1, 3.2, 3.3 and 3.4, and briefly described in the
404 following paragraphs.

405 Bio-profiler #1, launched in late October 2011 in the centre of the deep water recirculation just
406 east of Kerguelen Island, initially encountered cold, well oxygenated waters with moderate biomass
407 ($T \sim 3$ °C, $O_2 \sim 330$ µmol kg^{-1}, 0.5 µg L^{-1} < Chl-a < 2 µg L^{-1}; profiles 1-90, Nov.). It was then carried
408 north-eastward across the Gallieni Spur where it encountered warmer waters with extremely high
409 biomass ($T \sim 5$ °C, chlorophyll up to nearly 10 µg L^{-1}), which satellite ocean colour animations
410 suggest was being swept northward as a mix of waters from the northern and central regions of the
411 Kerguelen plateau (see the animation "bloom 2011" in supplementary material; Trull et al, 2015).
412 During the subsequent southward transport, it crossed the Polar Front near 51.5° S, as shown by the
413 presence of a temperature minimum near 150 m depth ($T \sim 1$ °C; profiles ~ 200-220, end of Jan.).
414 The shoaling of low dissolved oxygen layers in this region provides another indication of their
415 Antarctic Zone oceanographic classification. Surface waters above this remnant winter water were
416 relatively warm despite deep mixed layer depths (~ 100 m, $T > 6$ °C; profiles ~240-330, Feb.-Mar.).
417 Much of this warming is probably seasonal, as these waters were encountered in late summer, but the
418 co-occurrence of somewhat elevated salinity (~ 33.8) suggests that flow of Polar Frontal Zone surface
419 waters over the Antarctic waters was also involved. During the February bio-profiler transit, these
420 waters exhibited only low to moderate chlorophyll biomass (~1.5 µg L^{-1}), although satellite images
421 suggest higher concentrations (~3 µg L^{-1}) were present earlier in December and January (see Figures
422 1b and 1c and the animation "bloom 2011" in supplementary material; Trull et al., 2015). The

423 particulate backscattering signal reflected the chlorophyll evolution along most of the trajectory,
424 except in January when, as the chlorophyll levels decreased (from >3 μg L^{-1} to ≤ 2 μg L^{-1}), b_{bp}
425 remained high and constant (-2.5 m^{-1} ≤ log(b_{bp}) ≤ -2.0 m^{-1}), suggesting detrital particles developed
426 from the high chlorophyll biomass, or possibly a (relatively large) change in chlorophyll/particulate
427 organic carbon ratio (Chl/POC) due to phytoplankton community composition. Finally, after 300
428 shallow profiles, bio-fouling of the fluorescence and particulate backscattering sensors marked the
429 end of their utility, as shown by the occurrence of elevated and highly noisy values throughout the
430 water column (see Figure 3.1c and e).

431 Bio-profiler #2, launched in late January 2014 south and east of the recirculation feature, initially
432 encountered Polar Frontal Zone waters which were present further south in this region than during
433 the 2011 year sampled by bio-profiler #1. For approximately the first 150 profiles, these waters
434 displayed relatively homogenous, moderately warm temperatures (4-5 °C) that continued to warm to
435 ~6 °C through February. The bio-profiler then transited much further south, briefly encountering
436 waters with strong shoaling of subsurface salty, low oxygen characteristics around profiles 160-170
437 (S ~ 34.0-34.2, O_2 ~ 260 μmol kg^{-1}), and entered colder Antarctic waters where it remained through
438 profile ~220, at which time its return north brought it back into Polar Frontal Zone waters showing
439 autumn cooling. Throughout its life, in comparison to bio-profiler #1, only low-to-moderate biomass
440 waters were encountered (<1.5 μg L^{-1}), though these values were persistently above Southern Ocean
441 HNLC background values (< 0.5 μg L^{-1}). Within this range, the higher biomass values, which also
442 extended over greater vertical extents (~ 100 m), were found in the Antarctic waters (profiles 170-
443 250, Mar.-Apr.). In contrast, the higher b_{bp} values were found at the beginning of the trajectory
444 (log(b_{bp}) ~ -2.5 m^{-1}), and their deep extent and high values compared to chlorophyll levels suggest
445 the existence of higher chlorophyll concentrations prior to the bio-profiler deployment. This is in
446 agreement with satellite ocean colour animations on which high biomass development is observed in
447 December 2013 in the area of the bio-profiler deployment (see Figures 1e and 1f and the animation

448 "bloom 2013" in supplementary material). After this initial difference, the b_{bp} variations followed
449 those of chlorophyll along the rest of the trajectory.

450 Bio-profiler #3, launched in late January 2014 in the northern portion of the recirculation feature,
451 followed a similar trajectory to that of bio-profiler #1 launched in October 2011 and encountered
452 much warmer waters with similar mixed layer depths, between 40 and 70 m (Figure 3.3). Presumably
453 this represents seasonal warming as salinities were similar to those encountered in spring (~ 33.85),
454 and the warming from ~3 °C to nearly 6 °C is consistent with seasonal warming amplitudes observed
455 in satellite surface temperature records for unfertilized open ocean Polar Frontal Zone waters (Trull
456 et al., 2001). Persistent high chlorophyll levels were also observed initially in the recirculation region
457 (up to ~4 versus ~1 µg L^{-1}), but the float did not cross the Gallieni Spur (GS in maps of Figure 3)
458 where bio-profiler #1 encountered values up to nearly 10 µg L^{-1}. During its transit south near 75° E,
459 only Polar Frontal Zone waters were encountered, and chlorophyll levels remained moderately high
460 (between 1 and 2 µg L^{-1}). At the beginning of the trajectory, the particulate backscattering b_{bp} signal
461 evolved in concert with the chlorophyll signal, but with a ~ 7-10 day delay. Another difference
462 between the two biomass parameter evolutions was the large increase of b_{bp} compared to chlorophyll
463 between the surface and 100 m, right after the profiler turned southward in the vicinity of the Gallieni
464 Spur (~ profiles 190-205, end of March).

465 Bio-profiler #4, deployed well east of the recirculation feature in early February, was initially in
466 warm, quite salty and well oxygenated waters, characterized by moderate biomass (first 80 profiles:
467 T ~ 5.5 °C, S ~ 33.8, O_2 ~ 310 µmol kg^{-1}, Chl-a < 1.5 µg L^{-1}, log(b_{bp}) ~ 3.35 m^{-1}). As its trajectory
468 approached the Gallieni Spur, surface waters became progressively warmer, fresher and less
469 oxygenated (profiles 80-250: T ~ 7 °C, S ~ 33.7, O_2 ~ 290 µmol kg^{-1}). During this time, the bio-
470 profiler recorded high chlorophyll and particle concentrations (chlorophyll values reaching up to 3
471 µg L^{-1} for profiles 80-130). This high biomass could be a remnant of the rich filament that transited
472 in this area a month prior to the visit of the bio-profiler (see the animation "bloom 2013" in
473 supplementary material). As the bio-profiler drifted further east, it was entrained in a relatively

stationary cyclonic eddy where it performed several loops before exiting to the south (profiles ~ 130-240, mid-March – mid-April). This eddy can be identified from altimetry as retentive – i.e. capable of entraining Lagrangian particles for, in this case, a few weeks to one month (d'Ovidio et al., 2013; Figure 8b). While retained by this mesoscale eddy, the bio-profiler measured a relatively constant profile of temperature and salinity, with slowly decreasing Chl-a concentrations and b_{bp} (Figure 8). Relatively constant hydrological properties throughout this period and the repeated looping suggest a largely Lagrangian trajectory within a single water parcel at this time. Of all the observations, this region displayed surface waters with the highest temperatures and lowest salinities (T ~ 8.0 °C, S ~ 33.6).

4 Discussion

With this overview of the spatial and temporal characteristics of our observations in hand, we proceed to evaluate our research questions.

4.1 Do the satellite images of surface chlorophyll reflect water column contents?

As discussed in the Introduction, it is important to determine whether the water column information provided by the bio-profilers changes perspectives on the mesoscale distributions of chlorophyll as seen in satellite images (Figure 1) This is a larger issue than whether our in-situ measurements of surface values differ from satellite values. We did not evaluate that question owing to extensive cloud cover greatly limiting match-ups between bio-profiler and satellite observations, and because we know that both our sensor calibrations and the satellite algorithms have large uncertainties (see the Methods sections 2.2 and 2.3). Instead, we examined the bio-profiler water column observations to determine what biases might be expected from observing only their upper portions, i.e. as a satellite would. There are two aspects of this issue that we could readily address: i) were subsurface chlorophyll maxima commonly present below the depth of satellite observation, and

498 did they vary spatially or temporally? ii) were surface chlorophyll values linearly and tightly
499 correlated with water column inventories with similar dynamic ranges, or were surface values poor
500 guides to water column inventories? We address these issues in this order in the following paragraphs.

501 Our statistics on the occurrence of subsurface chlorophyll maxima (Table 3) show that these
502 features were present in a significant fraction of the profiles (up to 14% of the night profiles and up
503 to 21% of the quenching-corrected day profiles). They mostly occurred at depths greater than the
504 MLD (Table 3) and, thus, too deep to be taken into account in the satellite observations. Without
505 radiation sensors on the bio-profilers, the first penetration depth (z_{pd}, light attenuation by 1/e) that
506 characterizes satellite observations could not be directly estimated, but based on the model of Morel
507 and Maritorena (2001; their figure 6), and using the relationship $z_{pd} = z_{eu}/4.6$ for the euphotic zone
508 definition of the 1% photosynthetically active radiation level (Gordon and McCluney, 1975), it was
509 at most 10-15 meters, and thus always within the mixed layer. Thus, we focused on these subsurface
510 maxima occurring below the MLD (hereafter $SubMax_{>MLD}$) and we examined the location of the
511 profiles exhibiting these features as well as their associated depth (see Figures 4a, 4b, 4d and 4e).

512 These $SubMax_{>MLD}$ were quite localized. They occurred primarily near the plateau or close to the
513 location of the Polar Front. Specifically, most of the profiles exhibiting this feature were found in the
514 vicinity of the steep slope between the Northern Kerguelen Plateau and the Gallieni Spur, between
515 40 and 80 m depth (Figures 4a, 4b, 4d and 4e). Occurrences of $SubMax_{>MLD}$ were much more sporadic
516 south of 50° S, on the south-eastward trajectories of bio-profilers #1 and #2. These conclusions about
517 the locations of subsurface chlorophyll maxima are similar for both night and day occurrences (stars
518 and open circles in Figure 4, respectively), although $SubMax_{>MLD}$ of day flagged profiles occurred
519 mostly at shallow depths (< 50 m, Figures 4b and 4d) and may result from an under-correction of the
520 surface quenched Chl-a concentrations (see Methods section 2.2). It seems that light limitation may
521 not be a major driver of subsurface Chl-a maxima via the mechanism of increased Chl-a production
522 per cell, at least under a certain threshold of Chl-a content, since $SubMax_{>MLD}$ observed by bio-
523 profilers #3 and #4 occurred more frequently when the mixed layer was deep (for 2.5 $\mu g\ L^{-1} \leq$ Chl-a

524 ≤ 5 µg L^{-1}; Figures 4c and 4f). However, the quasi-ubiquitous concomitance of $SubMax_{>MLD}$ for bio-
525 profiler #1 with shallow mixed layers, less than 50 m, suggests that above a certain threshold of Chl-
526 a content, self-shading may promote pigment production by phytoplankton at depth.

527 Subsurface chlorophyll maxima beyond the reach of satellite imagery can be thought of as a
528 specific class of the wide range of possible chlorophyll distributions (such as varying thicknesses of
529 relatively constant near-surface biomass layers, or changes in the rate of decrease of biomass with
530 depth) that could introduce bias between surface concentration and water column inventory
531 perspectives. To gain perspective on the overall importance of these possibilities, we compared
532 surface chlorophyll concentrations measured by the profilers (using the shallowest ~10 m depth
533 observation since this was reliably within both the 1/e satellite ocean colour penetration depth and
534 the mixed layer) with their column inventories calculated from all observations in the top 200 m
535 (since chlorophyll distributions generally reduced to background values below this depth). These
536 comparisons, shown in Figure 5a (left column), display reasonably linear relationships over almost
537 the entire range of both night and daytime observations. This was especially true for bio-profilers #1
538 and #3 (correlation coefficients r^2=[0.60-0.85]), which include high chlorophyll values (greater than
539 2 mg m^{-3} for the surface concentration and greater than 160 mg m^{-2} for the 0-200 m inventory). Most
540 of the flagged daytime profiles (red circles in Figure 5a) seem to be shifted slightly left of the linear
541 regression lines, suggesting that they may well represent under-corrected quenched chlorophyll rather
542 than true features. Overall, qualitatively, these quite linear relationship between surface Chl-a
543 concentration and 0-200 m integrated Chl-a content suggests that satellite observations are reasonably
544 good indicators of the spatial distributions water column chlorophyll inventories.

545 Concerning the particulate backscattering signal, the linear correlations between surface values
546 and inventories were generally not as strong as for Chl-a, except for bio-profiler #3, as shown in
547 Figure 5b (right column: r^2 = [0.29-0.74]. It appears that surface b_{bp} values lower than ~2 x 10^{-3} m^{-1}
548 vary similarly to the 0-200 m b_{bp} inventories, whereas higher surface values exhibit noisier

549 correlations when compared to the 0-200 m integrated b_{bp} contents (see the slope breaks in the
550 relationship between surface and 0-200 m integrated b_{bp} in Figure 5b). The origin of this non-linearity
551 is not clear, and its evaluation is potentially compromised by the spikiness of the b_{bp} records and their
552 poor vertical resolution. The particulate backscatter profiles (Figures 2b, 3e and 9e) suggest that
553 spikes may be particularly common at the base of the mixed layer and below, and thus might reflect
554 differential control of phytoplankton and total particle populations. Future deployments with
555 improved firmware to yield higher resolution may be able to advance the interesting possibility that
556 backscatter information can provide ecosystem perspectives beyond phytoplankton biomass alone.

557 Because our qualitative assessment indicated that surface Chl-a concentrations provide a
558 relatively unbiased indication of the water column Chl-a inventory, we now try to go a little bit further
559 towards a quantitative assessment of possible biases between satellite and in-situ Chl-a perspectives.
560 First, we compared the coefficients of variation (i.e. the ratio of the standard deviation to the mean)
561 of the surface chlorophyll concentrations and of the water column inventories. Using only the night
562 data to avoid quenching correction uncertainties, surface distribution coefficients of variation (#1:
563 82%; #2: 20%; #3: 39%; #4: 43%) revealed very similar relative dispersions to the water column (0-
564 200 m) inventory coefficients of variation (#1: 84%; #2: 20%; #3: 34%; #4: 31%). Thus, satellite
565 images reasonably reflect the relative range of mesoscale variability in water column phytoplankton
566 biomass accumulations. Surprisingly, surface chlorophyll values (i.e. satellite images) would tend to
567 slightly overestimate the relative dispersion of Chl-a data for bio-profilers #3 and #4, despite those
568 profiles exhibiting the largest numbers of night subsurface maxima (in %, Table 3). This means that
569 the association of high surface chlorophyll concentrations with shallow chlorophyll layers was more
570 important than the presence of subsurface chlorophyll maxima in determining the relationships
571 between surface and water column inventories.

572 To further explore this issue, we calculated expected water column inventories for chlorophyll
573 layers confined to the physical mixed layer depths at the time of observation (by multiplying each
574 surface concentration by its associated mixed layer depth, MLD). This is akin to trying to improve

575 satellite assessments using mixed layer depth information from, for example, standard ARGO floats
576 that measure only temperature and salinity. These comparisons are shown in Figure 6a and reveal that
577 this approach badly underestimates water column inventories (at least with our MLD definition) and
578 that this underestimation is very common. Most of the "0-200 m integrated Chl-a/(surface Chl-a ×
579 MLD)" ratios range from 1/1 to 4/1, with a few profiles of bio-profilers #1 and #3, at the time when
580 they recorded the highest bio-optical values, reaching ratios of 20/1 (profiles ~ 70-130 for bio-profiler
581 #1 and profiles ~ 0-70 for bio-profiler #3). Moreover, the colour coding in Figure 6a shows that this
582 bias is strongest for shallow mixed layers in general. In other words, the presence of significant
583 amounts of chlorophyll below the mixed layer is very common (though generally not as local vertical
584 chlorophyll maxima, for which our statistics confine the occurrence of those exceeding 60% of
585 surface to 17% of the sampled locations and those exceeding 100% of surface to 11% of the sampled
586 locations). Notably, this bias still persists strongly if we change our MLD definition to the much
587 larger criterion of Levitus (1982; density increase of 0.125 kg m^{-3} relative to the density at 0 m). For
588 this criterion, the (surface Chl-a × MLD) estimation ranged between half and twice the 0-200 m
589 integrated Chl-a content for MLD deeper than 60 m (close to half for MLD ~ [60-90] m and surface
590 Chl-a < 2 µg L^{-1} to close to twice for MLD > 120 m and surface Chl-a > 2 µg L^{-1}). However, (surface
591 Chl-a × MLD) estimations were still twice to four times lower than the 0-200 m integrated Chl-a
592 content recorded by the bio-profilers when the MLD ranges between 40 and 60 m (not shown).

593 The most probable explanation for these observations is that the mixed layer at the time of
594 observation was shallower than at the time of generation of the biomass. This is of course expected
595 as a result of seasonal shallowing of the mixed layer, but the magnitude of the effect is important to
596 recognize (as we have shown above) it is well above what could be corrected using some other mixed
597 layer depth criterion. Interestingly, there appears to be a relatively simple hyperbolic relationship
598 between the ratio "0-200 m integrated Chl-a" / "surface Chl-a × MLD" (hereafter designated as X)
599 and MLD, as shown in Figure 6b for the MLD definition of Park et al. (1998). It also holds for the

MLD definition of Levitus (1982). This X vs MLD hyperbola reaches an asymptote of X ~ 1 for MLD values close to the 150-200 m depths of regional winter mixed layers (visible as temperature minima remnant signatures of winter cooling in profiles south of the Polar Front in Figure 3b). Moreover, the curve is reasonably well parameterized by $X \sim MLD^t/MLD^w$, in which the superscripts t and w indicate mixed layer depths at the time of observation and the end of winter, respectively. This relationship could arise if most biomass accumulation occurred in early deep mixed layers with subsequent stratification adding little additional biomass, or if mixed layers shallowed and deepened episodically as biomass accumulation developed throughout the season.

Overall, these results emphasize the major challenges that are present for connecting surface chlorophyll distributions to total water column biomass and primary productivity, since they reveal that physical mixed layer depths are often not a reliable guide to biomass distributions. These physical and biological responses seem to be modulated differently on diel, weather, and seasonal timescales, and are also affected by the mesoscale and sub-mesoscale interleaving of water parcels. The quantification of near surface mixing (i.e. going beyond the limited mixed layer depth concept) is currently under very active exploration and debate in the context of seasonal drivers of production (Behrenfeld, 2010; Taylor and Ferrari, 2011), and these data reveal the need to extend those perspectives to shorter time and space scales. The presence of significant amounts of chlorophyll below the mixed layer is also important to its ultimate fate –if this biomass is not re-entrained then it may well contribute preferentially to export and to mesopelagic oxygen consumption (issues which we revisit in Discussion section 4.3 below).

4.2 Do regions of high biomass correlate with (local) oceanographic properties?

To evaluate this issue, we examined bivariate regressions of Chl-a inventories (0-200 m) with physical water column characteristics, after having separated the observations into two groups: 1) Chl-a inventories > 200 mg m^{-2} in rich biomass regions close to the plateau, and 2) Chl-a inventories ≤ 200 mg m^{-2} in moderate biomass regions far from the plateau (the rich and moderate biomass

regions considered here are identified by red and yellow rectangles in Figures 3.1c, 3.2c, 3.3c and 3.4c). As shown in Figure 7 (a, b and c), the richest biomass regions encountered by bio-profiler #1 in 2011 and bio-profiler #3 in 2014 were associated with waters with very similar properties, specifically moderate temperatures (3.5-5 °C), high salinities (33.82-33.85), and thus relatively high densities (sigma-theta values of 26.7-26.9 kg m^{-3}). The bio-profiler #1 distributions of chlorophyll with these properties showed linear decreases on either side of these values, suggestive of mixing with surrounding waters much poorer in Chl-a. This characteristic is also observed between integrated Chl-a and mean surface oxygen saturation ($O_{2\ sat}$, Figure 7f), for which the high $O_{2\ sat}$ states (reaching 10% supersaturation) indicate oxygen production in these high biomass waters (since these values exceeding expected from processes such as warming or bubble injection; Shadwick et al., 2014). Relatively high biomass was also encountered in waters with extreme T-S properties (the warmest and freshest observed) in the vicinity of the Gallieni Spur by bio-profiler #4 (black symbols in Figure 7). Thus, there was not a unique class of waters with high biomass. This perspective is further reinforced by the lack of any clear relationships between chlorophyll inventories and local water column properties for regions of moderate biomass, including versus mixed layer depth and the intensity of stratification as represented by the Brunt-Väisälä frequency (Figure 7, right column). These low biomass waters also exhibited lower $O_{2\ sat}$ states (95-103%) than those of rich biomass areas. The under-saturated oxygen levels reflect either strong local respiration or the supply of low oxygen waters from below, with these processes difficult to distinguish (except for specific portions of the bio-profiler #4 trajectory where time series within constant physical property layers were obtained, as discussed in section 4.3).

Linking local water parcel properties to past water trajectories with respect to the Kerguelen Plateau, as a known natural source of iron fertilization, provides an additional view of the role of water mass properties in the control of chlorophyll inventories. For the richest Chl-a waters (T ~ 4 °C, S ~ 33.83, σ ~ 26.8 kg m^{-3}) encountered by bio-profiler#1, surface drifters released during the

KEOPS2 voyage (d'Ovidio et al., 2014) suggest these waters derive from the northern Kerguelen plateau. The computation of trajectories based on satellite altimetry (see Methods section 2.3) for all the bio-profilers confirms this perspective and also indicates that the time since a water mass left the plateau (Figure 8b) is another important determinant of chlorophyll levels (presumably as a result loss of Fe over time after its addition from the plateau; d'Ovidio et al., 2014). These results are shown in Figure 8. Figure 8 b) and d) compares water age and origin with the 0-200 m Chl-a inventories for spring (bio-profiler #1, in blue in the plots) and summer (bio-profilers #2, #3, #4, in black in the plots). Beside a strong seasonal difference –spring values range from up to 1000 mg m^{-2}, whereas in the summer few measurements exceed 300 mg m^{-2}– water parcels corresponding to high Chl-a inventories appear to be waters that have recently left the Kerguelen Plateau (20-40 days of water age; Figure 8a) and come generally from its northern part ([-49; -47] °S; Figure 8c). Bio-profilers locations that correspond to water parcels that have not touched the Plateau in the last 100 days (points shown in white for water age = 100 in Figure 8b) do not present any high integrated Chl-a values, suggesting that the main source of iron fertilization for the explored water masses is horizontal advection from the Kerguelen Plateau. This correlation of high Chl-a inventories with age since leaving the plateau is unlikely to be biased by the lower frequency of sampling (shown in the Figure 8b inset) of older waters, given that a statistical test based a 10^4 samplings of a uniform distribution of integrated Chl-a at the sampling frequency of each water age yielded a probability (p) of not-sampling integrated Chl-a value greater than 200 mg m^{-2} for water parcels with water ages greater than 40 days of $p < 10^{-4}$.

These results suggest that the northern Kerguelen Plateau is an important target region for future studies of iron delivery mechanisms into the plume downstream. In terms of the secondary influences of mixed layer depth and stratification, the bio-profiler #1 profiles with integrated Chl-a greater than 600 mg m^{-2} were mainly characterized by a shallow mixed layer, lower than 60 m (Figure 7d), and a low stratification ($-0.01\ s^{-2} < \max N^2 < 0\ s^{-2}$; Figure 7e). Below this Chl-a inventory threshold, no clear relationships emerged between MLD or N^2 and 0-200 m integrated chlorophyll (Figures 7d and

676 7e). In a steady state perspective, this lack of correlation could arise because mixed layers were
677 shallow enough that light limitation was not sufficient to halt phytoplankton accumulation, yet not so
678 shallow that mean mixed layer light levels allowed light promoted growth to reach accumulations
679 that became self-shading (viewpoints that have been developed previously, based on relationships
680 between fluorescence and mixed layer depth observations in this region using sensors on elephant
681 seals; Blain et al., 2013). Importantly, our observations emphasize that chlorophyll distributions do
682 not track the shoaling of mixed layer depth on seasonal or weather timescales, and thus that MLD
683 variability is unlikely to show simple relationships to biomass accumulation. This point has also been
684 emphasized in terms of competing effects of light and Fe limitation responses to MLD variability
685 (Joubert et al., 2014), for waters where vertical Fe supply is dominant (rather than the horizontal
686 dominance of supply studied here).

687

688 ***4.3*** **Can the fate of surface enrichments in biomass be determined, and if so, what is the**
689 **percentage of biological production exported?**

690 Evaluating this question requires the extraction of a temporal perspective from the bio-profiler
691 records, and is thus only possible for portions of their trajectories which appear to be essentially
692 Lagrangian. The best record for this approach is for bio-profiler #4 during the period when it carried
693 out several clockwise loops in late autumn, i.e. for profiles 150-240 (Figure 3.4a). During this time,
694 its trajectory was very similar to that expected based on surface currents estimated from satellite
695 altimetry, the density stratification of the water column was relatively steady, and the T-S profiles
696 were tightly grouped (Figures 9b, 9c and 9d). These observations suggest that the profiler remained
697 within a single water parcel, that was entrained by a retentive eddy and underwent only small
698 exchanges with surrounding waters, as shown by slightly warmer (profiles 165-170 and 200-220) and
699 cooler (profiles 175-195) conditions along the trajectory (these are discussed further below).

At the start of this period (blue lines subset in Figure 9e), chlorophyll profiles showed moderate to high surface and subsurface layer levels, well above HNLC background values, with some profiles exhibiting subsurface maxima reaching up to 1.5 μg L^{-1} between 50-70 m depth and up to 1 μg L^{-1} around 120 m depth. Both the surface constant Chl-a layer and the subsurface "chlorocline" layer (by analogy to thermocline or halocline, "chlorocline" is defined here as the depth range with the highest chlorophyll concentration gradient) were thick, equal to ~ 80 m and ~50 m, respectively. The origin of the smaller and variable subsurface maxima seen in some profiles in Figure 9e is uncertain. One possibility is that they are remnants of the high surface chlorophyll biomass observed just prior to the eddy entrapment (visible in Figure 3.4c and the "bloom 2013" animation in the supplementary material), that had been carried to depth by particle settling or by subduction of the denser, saltier, and slightly cooler water associated with that high biomass. Associated b_{bp} profiles showed similar large variations with strong local maxima correlated to local Chl-a maxima (blue lines subset in Figure 9f). The strong variability of the Chl-a/b_{bp} profiles over the first 100 m suggests possible changes in the composition of the particulate assemblage (blue lines subset in Figure 9g).

During the Lagrangian eddy entrapment period, the surface mixed layer chlorophyll levels declined further from 1.5 μg L^{-1} to ~1 μg L^{-1} (Figure 3.4c and 9e). Since the constant chlorophyll surface layer shallowed progressively with time, this Chl-a decrease did not result from the possible effect of dilution by mixed layer deepening (i.e. entrainment). Furthermore, the chlorocline content decreased briefly before re-increasing progressively in its upper part, and then its deeper part. In parallel, b_{bp} and Chl-a/b_{bp} profiles became tighter and tighter (light blue to orange profiles in Figures 9f and 9g) before re-exhibiting larger variations (red profiles). These results suggest the possibility of some chlorophyll conversion to non-fluorescent material, or its removal by export to depth or by local respiration or both, throughout the eddy entrapment. They may also of course partly reflect small spatial variations in the structure of the biomass distributions.

To evaluate these possibilities we examined changes in three layers, the surface layer (labelled layer 1 and defined as the surface down to the 26.6 isopycnal surface), and two density layers

immediately below it (layers 2 and 3, respectively for density ranges 26.6-26.8 and 26.8-26.9). In order to characterize the existence of vertical or horizontal mixing during the eddy entrapment, mean temperature, salinity, depth of the density layers, as well as their thickness and their stratification state, are shown in Figure 10 (a, b, and c). The thickness and mean depth of the surface density layer were relatively constant in the first half of the eddy entrapment, then slightly increased as some warmer and fresher - thus lighter - water entered into the eddy structure (profiles 200-220). Contrastingly, the physical properties of the two deeper underlying density layers showed insignificant temporal trends and smaller variability over the period of interest, and thus changes in their biogeochemical properties can be attributed to local processes rather than exchanges.

The evolution of chlorophyll, particulate backscattering and dissolved oxygen inventories also exhibited different trends and variability for each layer (as shown in Figure 10d, e and f). In surface layer 1, mean chlorophyll and b_{bp} showed no overall temporal trend (green and grey curves in Figure 10d, respectively), although characterized by two maxima, one at the beginning of the eddy and one coinciding with the fresher warmer water occurrence described above. The oxygen content continuously decreased steadily until after profile 200, when larger variations were observed, with a minimum content coinciding with the fresher warmer waters. Within the underlying layer 2, chlorophyll, b_{bp} and oxygen inventories showed similar evolutions: all had maximums at the beginning of the eddy and then decreased with time until the bio-profiler exited the eddy (Figure 10e). These characteristics were also present in the deepest layer 3, although with significant differences in the magnitudes of change, specifically the oxygen decrease was similar to that of layer 2, but the chlorophyll level and its absolute magnitude of decrease were much smaller, and the b_{bp} levels remained relatively high for a longer portion of the record.

To verify that these changes were oceanographic, we again evaluated fluorometer and oxygen sensor drifts, but this time only over the range of profiles considered for the eddy entrapment investigation (following the approach used in Table 2, of examining the evolution of the mean values

751 within the depth layer 950-1000 m). Chl-a and O_2 drifts were respectively estimated to be +0.017 µg
752 L^{-1} and +1.05 µmol kg^{-1}.Thus, the temporal drifts probably lead to underestimations of the observed
753 decrease of Chl-a (of ~7% in layer 2 and of ~ 20% in layer 3) and of O_2 (~30% in layers 2 and 3).
754 Knowing that excluding the contribution of the drifts would only reinforce the trends described above,
755 we can now suggest the following overall interpretation to explain these variations of Chl-a, b_{bp} and
756 O_2 in these 3 density layers during the eddy entrapment of bio-profiler #4. In the surface layer 1, the
757 chlorophyll inventory seems to result from the combination of local biological processes with weak
758 horizontal resupply from warmer, fresher, and less oxygenated water (Figures 9a and 9d). In the
759 middle density layer 2, where mixing is considered insignificant because of the tightly grouped T-S
760 properties, the chlorophyll decrease does not seem to be due to local transformation to non-fluorescent
761 detritus since no corresponding increase in the b_{bp} signal was observed (Figure 10e). This leaves loss
762 by settling or respiration as possible explanations. Loss by settling is certainly possible on this
763 timeframe (rates of only a few meters per day are required), and the high b_{bp} values found in the lower
764 density layer 3 around profiles 160-180 could reflect transfer from the overlying layer 2. Biomass
765 loss by respiration and remineralization to dissolved inorganic carbon is almost certainly also
766 occurring given the decreasing oxygen inventories of the middle layer 2 and deep layer 3. For both
767 these layers the rate of chlorophyll loss is too small (by factors of 2-3, assuming a moderately high
768 phytoplankton C/Chl-a ratio of 50) to explain all the oxygen decrease, implying that degradation of
769 detritus (represented by the decreasing particulate backscattering signal) and dissolved organic matter
770 probably also contributes (this remains true even if we use a very high phytoplankton C/Chl-a ratio
771 of 100; Cloern et al., 1995). For the deepest layer 3, remineralization of settling particles coming from
772 above with a minor remineralization of local chlorophyll may best explain the slower decrease of
773 chlorophyll in comparison to that of oxygen.

774 In combination, these results suggest that not all of the accumulated biomass was respired in the
775 surface layer, with the CO_2 then returned to the atmosphere, and thus that there was some export.
776 Quantifying this export amount is difficult and merits a modelling and sensitivity assessment that is

beyond the scope of this paper. Here we simply provide an indication of its possible magnitude by comparison of the rates of mean oxygen loss in the surface layer 1 (representing carbon likely to be returned to the atmosphere) versus the subsurface layers 2 and 3 (representing carbon which may be exported in the ocean interior). The linear fits to the oxygen decreases for layers 1, 2, and 3 (as shown in Figure 10) imply oxygen consumption rates of approximately 5, 4, and 4 µmol m^{-3} d^{-1}, respectively. These values lie towards the lower end of estimates for annual rates at mesopelagic depths (Sarmiento et al., 1990). Comparing O_2 consumption of layers 2 and 3 (by multiplying the O_2 consumption rate by the thickness and the average density of the layer) relative to the total mean consumption among the three layers, we estimate that 35% of the CO_2 produced during this autumn period of bloom decline was exported from the surface layer (with 20% respired within layer 2 and 15% within layer 3). An analogous area of low-to-moderate production and relatively high export was observed during the KEOPS2 field cruise just south of Polar Front, in a meander area around 72.5° E – 49° S where the flow – considered as Lagrangian – was sampled in few stations as a time series (Laurenceau-Cornec et al., 2015; Planchon et al., 2014). This area coincides with the location of the anti-cyclonic trajectory of bio-profiler #3, around profile #110, where moderate biomass production was observed (Figure 3.3c), although spatial variations in this region unfortunately precluded estimation of biologically driven oxygen consumption from the bio-profiler.

5 Conclusions

The bio-profilers revealed several interesting aspects of the enriched biomass plume downstream from the Kerguelen plateau, by providing observations of its vertical dimension. First of all, the observations show that surface and total water column chlorophyll inventories are generally well correlated, which suggests that satellite perspectives on bloom spatial dynamics (e.g. Mongin et al., 2008; 2009) are unlikely to be strongly biased. This result holds true despite the presence of moderate

(60% above surface values) subsurface chlorophyll maxima in up to ~20% of all the profiles, and strong (100% above surface values) in ~10% of all the profiles (Table 3 and Figure 4). Furthermore, satellite surface observations seem to well reflect the water column relative range of mesoscale variability in biomass accumulations. However, the retrieval of water column Chl-a inventory from satellite surface observations is not simple. The bio-profilers often recorded significant quantities of biomass below the diel mixed layer, potentially correlated to the degree of shallowing of the mixed layer from deep winter values. The mixed layer at the time of the observations may not be the best parameter to quantify the chlorophyll inventories, especially when stratification by advection of lighter water mass or by seasonal warming creates strong density variations in the upper layer and, thus, shallow mixed layers, and considering that chlorophyll production may have occurred much earlier than at the time of the observations. And of course, our work does not imply that satellite chlorophyll estimates are necessarily accurate. That is an issue which our data cannot address owing to the imprecision of the bio-optical sensors and the absence of calibration against local chlorophyll observations, an approach which recent work has shown to be necessary for satellite estimates as well (Johnson et al., 2013).

The occurrence of moderate subsurface chlorophyll maxima in our data (17%) was higher than for results obtained with fluorescence sensors deployed on elephant seals around the Kerguelen plateau (~9% using a criterion of 30% excess over surface values to define the maxima; Guinet et al., 2012). This may reflect the greater proportion of observations in the southern portion of the plume in the Guinet et al. (2012) study, a region where we also found that subsurface maxima were less common (~4% of profiles for bio-profiler #2 for our moderate criterion of 60% excess, Table 3, and ~6% using their 30% criterion, data not shown). Subsurface maxima were also uncommon well downstream to the east of the Kerguelen plateau. This is interesting in that it suggests that subsurface iron levels supplied by upwelling or vertical mixing were insufficient to drive biomass accumulations at the base of the mixed layer, or at least were less important than horizontal supply of Fe in surface waters. This is in contrast to Polar Frontal Zone waters much further to the east south of Australia

where persistent subsurface maxima have been observed (Parslow et al., 2001), and with observations from other autonomous profiling floats elsewhere in the Southern Ocean in which small subsurface maxima were found to be common in summer below the mixed layer (Carranza et al., 2014). Variations in the relative intensities of surface and deep iron supplies is a possible cause of these variations, but other processes may also be involved. As an example, the origin of the relatively more common and stronger subsurface chlorophyll maxima near the Gallieni Spur is not clear. Settling of surface biomass generated earlier in the season (Figure 1) and/or seasonal depletion of iron in surface waters which reduces phytoplankton growth rates are possibilities, but they cannot be assessed given our lack of early seasonal observations. A third possibility of the overlaying of low density waters southward across the Polar Front appears less likely, given that shipboard observations during KEOPS2 found that this process generated shallow high biomass layers (at the Polar Frontal stations F-L, TEW-7, and TEW-8; (Lasbleiz et al., 2014; Trull et al., 2015).

Our initial research goals included looking for oxygen supersaturations in deep chlorophyll maxima to estimate net community production (Spitzer and Jenkins, 1989), but this could not be achieved owing to confounding effects on super-saturations from strong mixing with higher productivity overlying waters, and on aliasing of daily cycles by internal waves (Park et al., 2008a). Thus our results cannot address the issues of whether productivity in subsurface layers may partly explain offsets between satellite and in-situ estimates of the Southern Ocean biological pump (Schlitzer, 2002) or whether the phytoplankton that grow in deep chlorophyll maxima are preferential contributors to carbon export (Kemp et al., 2000; Queguiner, 2013). We were able to make a first simple assessment of subsurface autumn oxygen consumption during the portion of the bio-profiler #4 trajectory that delivered a quasi-Lagrangian time series, and this provided the very useful result that approximately 35% of the biomass respiration in that period occurred beneath the mixed layer, and thus at depths favouring CO_2 export toward the ocean interior. This 35% can be approximately equated to an export/production "e-ratio" of 0.4, which is relatively high by global standards, but in

852 the middle of the large range of values observed in cold Southern Ocean waters (Maiti et al., 2013),
853 and similar to f-ratios estimated for high biomass waters over the central Kerguelen plateau in autumn
854 during the KEOPS1 campaign (Trull et al., 2008). Of course the subsequent fate of the exported CO_2
855 inferred from the bio-profiler #4 observations is uncertain, in that these waters were still within the
856 depth range of possible exposure to the atmosphere during later deeper winter mixing, although the
857 larger scale circulation in this region suggests it is a region dominated by subduction (Sallée et al.,
858 2010).

859 Our simple correlative evaluation of the bio-profiler observations of biomass variations
860 revealed that the highest chlorophyll levels were observed in surface waters with a narrow range of
861 densities and moderate temperatures (σ~26.9 ±.05 kg m^{-3}, T ~4 ±.5°C; Figure 7). This occurrence of
862 maximum biomass at moderate temperatures, along with the lack of correlation with mixed layer
863 depth (Figure 7) suggests that local controls on growth rates were less important than the history of
864 the levels of iron supplied in this water type. Notably, water with these properties was found
865 preferentially near the northern Kerguelen plateau and Gallieni Spur suggesting iron supply from this
866 region. This is consistent with geostrophic circulation estimates and a favourable wind regime for
867 upwelling in this region during the 2011 KEOPS2 period when bio-profiler #1 was deployed
868 (d'Ovidio et al., 2014; Gille et al., 2014) and with Lagrangian analyses that backtrack water parcels
869 to identify their origin. Further observations and analyses are of course necessary to determine the
870 generality of this inference that the northern Kerguelen plateau provides the major source of iron to
871 the downstream biomass plume. This is especially true given the limited seasonal and inter-annual
872 scope of our bio-profiler observations.

873

874 ***Acknowledgements***

875 This work was supported by the Australian Commonwealth Cooperative Research Program via the
876 ACE CRC. M. Grenier was supported by a conjoint LEGOS and ACE CRC postdoctoral appointment

and a CAMPUS FRANCE grant (FASIC award # 30418QG; campusfrance.org). A. Della Penna was supported by a conjoint Frontières du Vivant (Paris 7) and CSIRO-UTAS Quantitative Marine Science PhD scholarship. We thank Ann Thresher (CSIRO) for the harvesting and processing of the data from the bio-profilers, as supported by the Australian Integrated Marine Observing Argo and Southern Ocean Time Series facilities. We thank Cedric Cotté and Francesco d'Ovidio (LOCEAN, Universite de Paris VI) and the crew of the *RV Marion Dufresne* for bio-profiler deployments, and Stephane Blain and Bernard Quéguiner for KEOPS2 voyage leadership. Thanks to Vito Dirita, Alan Poole, and Craig Hanstein (CSIRO) for bio-profiler preparation, and Craig Neill and Kelly Brown (CSIRO) for oxygen optode calibrations. Thanks to Helen Phillips (IMAS) for fruitful discussions and advice concerning physical analyses of the hydrological variables, and Francesco d'Ovidio (LOCEAN, CNRS) for insights into Lagrangian perspectives on water parcel trajectories and their evolution. Finally, we gratefully acknowledge Dr S. Thomalla and an anonymous reviewer for their valuable comments on an earlier version of the paper that allowed us to improve it significantly.

List of Tables

Figure Captions

Figure 1. Maps of bio-profiler trajectories (white and grey lines) over remotely sensed chlorophyll-a distributions (a-h: daily, 4 km CLS/CNES product; i: weekly composite from GlobColour 4 km product). Top row: 2011 bloom season for bio-profiler #1. Middle and bottom rows: 2013/2014 bloom and beginning of post-bloom season for bio-profilers #2 (light grey trajectory), #3 (dark grey trajectory) and #4 (white trajectory). Red squares indicate the bio-profiler locations corresponding to the day of the image. The black thick line refers to the position of the Polar Front measured from hydrographic samples by Park et al. (2014a).

Figure 2. a) Assessment of bio-optical sensor stability from temporal evolution of chlorophyll and particulate backscattering values averaged over two depth ranges, 250-300 m (lines) and 950-1000 m (stars). Arrows indicate profiles considered to be affected by bio-fouling, which were not used in further analysis. b) Illustration of quenching corrections, showing pairs of successive night/day profiles (day: continuous lines; night: dashed lines). For each bio-profiler, the panel shows: chlorophyll profiles without quenching correction (left), chlorophyll profiles with quenching correction (middle), and associated particulate backscattering profiles (right). Squares in the middle panel represent threshold values of the lowest surface chlorophyll concentration for the night profiles of each bio-profiler (#1: 0.7 µg L^{-1}; #2: 0.4 µg L^{-1}; #3: 0.65 µg L^{-1}; #4: 0.7 µg L^{-1}). These threshold were used to flag day profiles having surface chlorophyll concentration still below this threshold after the quenching correction (see Table 3, Figures 4 (squares), 5 (red circles) and 7 (squares)), for which quenching might have been under-corrected. c) Comparison of bio-profiler #1 fluorescence Chl-a estimates to shipboard results obtained by the KEOPS2 project:, c.i. Location of KEOPS2 stations E1 (blue symbols) and E2 (black symbols) along a quasi-Lagrangian track followed by bio-profiler#1 (red symbols); c.ii Temperature profiles showing similar structures of the ship and bio-profiler sampled water columns; c.iii Fluorescence profiles (lines) showing that the

921 bio-profiler provided similar fluorescence results to the ship CTD mounted sensor, and that both
922 exhibited complex relationships to Niskin bottle total chlorophyll-a sample values (dots; see text for
923 further discussion).

924

925 Figure 3.1. Bio-profiler #1 observations

926 a) bio-profiler #1 trajectory over the bathymetry, with each point representing a depth profile and
927 the colour of the points changing from blue to red over time (dates are shown below the bottom
928 plots). The 700 m isobath is represented by the red line contour. KI = Kerguelen Island; KP =
929 Kerguelen Plateau; HI = Heard Island; GS = Gallieni Spur. b-f) Evolution of hydrological
930 parameters along the float trajectory: b) temperature (°C), c) chlorophyll (µg L^{-1}), d) salinity
931 (unitless), e) particulate backscattering (b_{bp}; log scale; m^{-1}), and f) dissolved oxygen (µmol kg^{-1}).
932 The white line represents the mixed layer depth. Red and yellow rectangles refer to rich and
933 moderate chlorophyll areas used in Figure 7 and discussed in Section 4.2.

934

935 Figure 3.2. Bio-profiler #2 observations (see Figure 3.1 caption for details).

936

937 Figure 3.3. Bio-profiler #3 observations (see Figure 3.1 caption for details).

938

939 Figure 3.4. Bio-profiler #4 observations (see Figure 3.1 caption for details).

940

941 Figure 4. Characteristics of subsurface chlorophyll maxima occurring at depths greater than the
942 mixed layer depth and exceeding the surface content by more than 60% (top) and 100% (bottom). a)
943 and d): geographical areas where these subsurface Chl-a maxima occur with an expanded view for

the Gallieni Spur region; b) and e): associated depths of these subsurface Chl-a maxima along the bio-profiler trajectories (i.e. versus profile numbers); c) and f): relationship between the amplitude of these Chl-a maxima (in $\mu g\ L^{-1}$) and the mixed layer depth (MLD, in m). Symbols: stars refer to night profiles, circles to day profiles and squares to flagged day profiles (i.e. which still exhibit, in the surface layer, a large concentration decrease toward low surface values that indicates the possibility of incomplete quenching correction; see definition in the caption of Figure 2b).

Figure 5. a) Surface chlorophyll concentrations (in mg m^{-3}) compared to chlorophyll inventories (0-200 m; in mg m^{-2}), for each bio-profiler. b) Surface particulate backscattering (m^{-1}) compared to particulate backscattering inventories (0-200 m), for each bio-profiler. Note that scales are slightly larger for bio-profiler #1 than for the others; the dashed rectangles in upper plots indicate the scales used for the other bio-profilers. Night profiles (black circles), day profiles (green circles) and potentially quenching under-corrected day profiles (red circles, flagged as defined in the caption of Figure 2b) are distinguished. Correspondingly, the green and black lines refer to the linear regression of day and night profiles, and their associated correlation coefficients, r^2.

Figure 6: a) Chlorophyll water column inventories (in mg m^{-2}), estimated by multiplying surface chlorophyll concentrations by the mixed layer depth, compared to chlorophyll inventories (0-200 m; in mg m^{-2}) recorded by the bio-profilers. Only night and unflagged day profiles are represented. The colour code shows the associated depth of the mixed layer (in m). The 5 lines $y = x$, $y = 2x$, $y = 4x$, $y = 8x$ and $y = 20x$ are given as indicators to quantify the ratio between the "surface Chl-a × MLD" product and the 0-200 m integrated Chl-a.

b) Representation of the X factor (X = (0-200 m integrated Chl-a)/(surface Chl-a × MLD)) as a

function of the mixed layer depth (in m), for the total data set. Symbols and colours are defined in the legend.

Figure 7. Relationship between 0-200 m integrated chlorophyll a concentration and various water properties for a-f) high biomass regions close to the plateau (bio-profilers #1 and #3) or entrapped in eddies (bio-profilers #2 and #4; red rectangles in Figures 3.1, 3.2, 3.3 and 3.4) and g-l) moderate biomass regions far from the plateau (yellow rectangles in Figures 3.1, 3.2, 3.3 and 3.4). a) and g): surface temperature (in °C); b) and h): surface salinity (unitless); c) and i): surface density (in kg m^{-3}); d) and j) mixed layer depth (MLD; in m); e) and k) maximum Brunt-Väisälä frequency squared (N^2; in s^{-2}) f) and l) oxygen saturation state (in %). Symbols and colours are defined in the legend.

Figure 8: Lagrangian diagnostics computed from altimetry. Maps of age and origins of the water parcels shown in plots (a) and (c) are from Figure 4 of d'Ovidio et al. (2014). White pixels represent water parcels that have not touched in the past 100 days the Kerguelen Plateau (defined by the 700 m isobath and shown in grey). Comparison of these age and origin metrics with the bio-profiler total integrated Chlorophyll-a values are shown in plots (b) and (d). Blue dots correspond to data collected during spring (bio-profiler #1, mean values in red) and black dots to data collected during summer (bio-profilers #2, #3, #4, mean values in magenta). White dots correspond to water parcels that have not touched the Kerguelen Plateau. The inset in plot b) shows the number of measurements for each water age. The black arrow highlights the fact that low Chl-a levels associated with water parcels that have not touched the Kerguelen Plateau within the last 100 days is supported by a large number of samples and, thus, seems to be a robust feature.

Figure 9. Eddy entrapment of bio-profiler #4.

a) Identification of entrapment along the bio-profiler trajectory, with the colour of the points changing, from blue to red over time, from profile 150 to profile 240.

b) Overlay of bio-profiler trajectory (white line) and eddy retention indices, showing the portion of the trajectory within a long-lasting (more than 30 days) retentive structure. The red square marks the temporal reference (profile 177) from which the Lagrangian trajectories were computed for the retention statistic, as described in Methods section 2.3.

c) Temperature-salinity diagram. Colours correspond to location on the map in a).

d) Temperature versus depth section with mixed layer depth (black line) and isopycnals indicated (white lines).

e) Chlorophyll profiles, coloured as on the map and separated, for the sake of clarity, in 4 subsets of ~23 profiles (equivalent to ~2 weeks of data acquisition).

f) As e), but for particulate backscattering (b_{bp}) profiles.

g) As e), but for the chlorophyll/b_{bp} ratio.

Note that chlorophyll and b_{bp} signals were filtered for visual clarity, using a 3 point running median.

Figure 10: Temporal evolution of physical and biological properties during the eddy entrapment of bio-profiler #4 for three density layers: with sigma-theta ranges of surface-26.6; 26.6-26.8; 26.8-26.9. Left column plots a-c) show physical properties: mean depth (in m; black line and scale), thickness (in m, dashed black line and black scale), temperature (θ, in °C; red line and scale), salinity (S, unitless; blue line and scale), density (σ, in kg m^{-3}; purple line and scale) and Brunt-Väisälä frequency squared (N^2, in s^{-2}; gray line and scale). Right column plots d-f) show biogeochemical properties: mean chlorophyll (Chl-a, in $\mu g\ L^{-1}$; green line and scale), particulate

backscattering (b_{bp}, in m^{-1}; gray line and scale), and oxygen concentrations (O_2, in μmol kg^{-1}; orange line and scale).

References

Assmy, P., Smetacek, V., Montresor, M., Klaas, C., Henjes, J., Strass, V. H., Arrieta, J. M., Bathmann, U., Berg, G. M., and Breitbarth, E.: Thick-shelled, grazer-protected diatoms decouple ocean carbon and silicon cycles in the iron-limited Antarctic Circumpolar Current, Proceedings of the National Academy of Sciences, 110, 20633-20638, 2013.

Babin, M., Morel, A., and Gentili, B.: Remote sensing of sea surface sun-induced chlorophyll fluorescence: consequences of natural variations in the optical characteristics of phytoplankton and the quantum yield of chlorophyll a fluorescence, International Journal of Remote Sensing, 17(12), 2417-2448, 1996.

Behrenfeld, M. J.: Abandoning Sverdrup's Critical Depth Hypothesis on phytoplankton blooms, *Ecology*, *91*(4), 977-989, 2010.

Biermann, L., Guinet, C., Bester, M., Brierley, A., and Boehme1, L.: An alternative method for correcting fluorescence quenching, Ocean Science, 11, 83–91, 2015.

Blain, S., Queguiner, B., Armand, L., Belviso, S., Bombled, B., Bopp, L., Bowie, A., Brunet, C., Brussaard, C., Carlotti, F., Christaki, U., Corbiere, A., Durand, I., Ebersbach, F., Fuda, J.-L., Garcia, N., Gerringa, L., Griffiths, B., Guigue, C., Guillerm, C., Jacquet, S., Jeandel, C., Laan, P., Lefevre, D., Lo Monaco, C., Malits, A., Mosseri, J., Obernosterer, I., Park, Y.-H., Picheral, M., Pondaven, P., Remenyi, T., Sandroni, V., Sarthou, G., Savoye, N., Scouarnec, L., Souhaut, M., Thuiller, D., Timmermans, K., Trull, T., Uitz, J., van Beek, P., Veldhuis, M., Vincent, D., Viollier, E., Vong, L., and Wagener, T.: Effect of natural iron fertilization on carbon sequestration in the Southern Ocean, Nature, 446, 1070-U1071, 10.1038/nature05700, 2007.

Blain, S., Queguiner, B., and Trull, T.: The natural iron fertilization experiment KEOPS (KErguelen Ocean and Plateau compared Study): An overview, Deep-Sea Research Part II-Topical Studies in Oceanography, 55, 559-565, 10.1016/j.dsr2.2008.01.002, 2008.

Blain, S., Renaut, S., Xing, X., Claustre, H., and Guinet, C.: Instrumented elephant seals reveal the seasonality in chlorophyll and light-mixing regime in the iron-fertilized Southern Ocean, Geophysical Research Letters, 40, 1-5, doi:10.1002/2013GL058065,052013, 2013.

Blain, S., Capparos, J., Guéneuguès, A., Obernosterer, I., and Oriol, L.: Distributions and stoichiometry of dissolved nitrogen and phosphorus in the iron-fertilized region near Kerguelen (Southern Ocean), Biogeosciences, 12, 623–635, 2015.

Boss E., and Pegau, W. S.: Relationship of light scattering at an angle in the backward direction to the backscattering coefficient, Applied Optics, 40(30), 5503–5507, 2001.

Boyd, P., LaRoche, J., Gall, M., Frew, R., and McKay, R. L. M.: Role of iron, light, and silicate in controlling algal biomass in subantarctic waters SE of New Zealand, Journal of Geophysical Research, 104, 13395-13408, 1999.

Boyd, P. W., Crossley, A. C., DiTullio, G. R., Griffiths, F. B., Hutchins, D. A., Queguiner, B., Sedwick, P. N., and Trull, T. W.: Control of phytoplankton growth by iron supply and irradiance in the subantarctic Southern Ocean: Experimental results from the SAZ Project, Journal of Geophysical Research, 106, 31573-31584, 2001.

Boyd, P. W., Jickells, T., Law, C. S., Blain, S., Boyle, E. A., Buesseler, K. O., Coale, K. H., Cullen, J. J., Baar, H. J. W. d., Follows, M., Harvey, M., Lancelot, C., Levasseur, M., Owens, N. P. J., Pollard, R., Rivkin, R. B., Sarmiento, J., Schoemann, V., Smetacek, V., Takeda, S., Tsuda, A., Turner, S., and Watson, A. J.: Mesoscale Iron Enrichment Experiments 1993-2005: Synthesis and Future Directions, Science, 315, 612 - 617, DOI: 610.1126/science.1131669, 2007.

Boyd, P. W., and Trull, T. W.: Understanding the export of marine biogenic particles: is there consensus?, *Progress in Oceanography*, *4*, 276-312, doi:210.1016/j.pocean.2006.1010.1007, 2007.

Boyd, P. W., and Ellwood, M. J.: The biogeochemical cycle of iron in the ocean, Nature Geoscience, 3, 675 - 682, 10.1038/ngeo964, 2010.

Carranza, M. M., Gille, S. T., Franks, P. J. S., Girton, J. B., and Johnson, K. S.: Mixed-layer depth and Chl-a variability in the Southern Ocean, ICES Journal of Marine Science, submitted, 2014.

Cavagna, A. J., Fripiat, F., Elskens, M., Dehairs, F., Mangion, P., Chirurgien, L., Closset, I., Lasbleiz, M., Flores–Leiva, L., Cardinal, D., Leblanc, K., Fernandez, C., Lefèvre, D., Oriol, L., Blain, S., and Quéguiner, B.: Biological productivity regime and associated N cycling in the vicinity of Kerguelen Island area, Southern Ocean, Biogeosciences Discuss., 11, 18073-18104, 2014.

Cetinić, I., Perry, M. J., Briggs, N. T., Kallin, E., D'Asaro, E. A., and Lee, C. M.: Particulate organic carbon and inherent optical properties during 2008 North Atlantic Bloom Experiment, Journal of Geophysical Research, 117, C06028, doi:10.1029/2011JC007771, 2012.

Cloern, J. E., Grenz, C., and Vidergar-Lucas, L.: An empirical model of the phytoplankton chlorophyll: carbon ratio-the conservation factor between productivity and growth rate, Limnology and Oceanography, 40, 1313-1321, 1995.

Constable, A. J., Nicol, S., and Strutton, P. G.: Southern Ocean productivity in relation to spatial and temporal variation in the physical environment, Journal of Geophysical Research - Oceans, 108, 8079, doi:8010.1029/2001JC001270, 2003.

Cullen, J. J.: The deep chlorophyll maximum: comparing vertical profiles of chlorophyll a, *Canadian Journal of Fisheries and Aquatic Sciences*, *39*(5), 791-803, 1982.

d'Ovidio, F., Della Penna, A., Trull, T., Nencioli, F., Pujol, I., Rio, M.H., Park, Y.H., Cott ,C., Zhou, M. and Blain, S. , The biogeochemical structuring role of horizontal stirring: Lagrangian perspectives on iron delivery downstream of the Kerguelen plateau, Biogeosciences Discussions, 2014.

d'Ovidio, F., De Monte, S., Della Penna, A., Cotté, C., and Guinet, C.: Ecological implications of eddy retention in the open ocean: a Lagrangian approach, Journal of Physics A: Mathematical and Theoretical, 46, 254023, 2013.

de Baar, H. J. W., de Jong, J. T. M., Bakker, D. C. E., Loscher, B. M., Veth, C., Bathmann, U., and Smetacek, V.: Importance of iron for phytoplankton blooms and carbon dioxide drawdown in the Southern Ocean, Nature, 373, 412-415, 1995.

Earp, A., Hanson, C. E., Ralph, P. J., Brando, V. E., Allen, S., Baird, M., Clementson, L., Daniel, P., Dekker, A. G., and Fearns, P. R.: Review of fluorescent standards for calibration of in situ fluorometers: Recommendations applied in coastal and ocean observing programs, Optics express, 19, 26768-26782, 2011.

Falkowski, P. G., and Kiefer, D. A.: Chlorophyll a fluorescence in phytoplankton: relationship to photosynthesis and biomass, Journal of Plankton Research, 7(5), 715-731, 1985.

Falkowski, P. G., and Kolber, Z.: Variations in chlorophyll fluorescence yields in phytoplankton in the world oceans, Australian Journal of Plant Physiology, 22, 341–355, 1995.

Fennel, K., and Boss, E.: Subsurface maxima of phytoplankton and chlorophyll: Steady‐state solutions from a simple model, Limnology and Oceanography, 48(4), 1521-1534, 2003.

Gille, S. T., Carranza, M. M., Cambra, R., and Morrow, R.: Wind-induced upwelling in the Kerguelen Plateau Region, Biogeosciences, 11, 6389–6400, 2014.

Goericke, R., and Montoya, J. P.: Estimating the contribution of microalgal taxa to chlorophyll a in the field-variations of pigment ratios under nutrient-and light-limited growth, Marine Ecology Progress Series, 169, 97-112, 1998.

1136 Gordon, H. R., and McCluney, W. R.: Estimation of the depth of Sun light penetration in the sea for
1137 remote sensing, Appl. Opt., 14, 413-416, 1975.

1138

1139 Guinet, C., Xing, X., Walker, E., Monestiez, P., Marchand, S., Picard, B., Jaud, T., Authier, M.,
1140 Cotté, C., and Dragon, A.-C.: Calibration procedures and first data set of Southern Ocean
1141 chlorophyll a profiles collected by elephant seal equipped with a newly developed CTD-
1142 fluorescence tags, Earth System Science Data Discussions, 5, 853-891, 2012.

1143

1144 Huot, Y., Babin, M., Bruyant, F., Grob, C., Twardowski, M. S., and Claustre, H.: Relationship
1145 between photosynthetic parameters and different proxies of phytoplankton biomass in the
1146 subtropical ocean, Biogeosciences, 4, 853–868, 2007.

1147

1148 Johnson, R., Strutton, P. G., Wright, S. W., McMinn, A., and Meiners, K. M.: Three improved
1149 satellite chlorophyll algorithms for the Southern Ocean, Journal of Geophysical Research-
1150 Oceans, 118, 1-10, 2013.

1151

1152 Jouandet, M.-P., Trull, T. W., Guidi, L., Picheral, M., Ebersbach, F., Stemmann, L., and Blain, S.:
1153 Optical imaging of mesopelagic particles indicates deep carbon flux beneath a natural iron-
1154 fertilized bloom in the Southern Ocean, *Limnology and Oceanography*, *56*(3), 1130-1140,
1155 doi:10.4319/lo.2011.56.3.1130., 2011.

1156

1157 Joubert, W., Swart, S., Tagliabue, A., Thomalla, S., and Monteiro, P.: The sensitivity of primary
1158 productivity to intra-seasonal mixed layer variability in the sub-Antarctic Zone of the Atlantic
1159 Ocean, Biogeosciences Discussions, 11(3), 4335-4358, 2014.

1160

1161 Kemp, A. E. S., Pike, J., Pearce, R. B., and Lange, C. B.: The 'Fall dump' - a new perspective on the
1162 role of a 'shade flora' in the annual cycle of diatom production and export flux, Deep Sea
1163 Research II, 47, 2129-2154, 2000.

1164

1165 Kiefer, D. A.: Fluoresence properties of natural phytoplankton populations, Marine Biology, 22,
1166 263–269, 1973.

1167

1168 Lasbleiz, M., Leblanc, K., Blain, S., Ras, J., Cornet-Barthaux, V., Hélias Nunige, S., and
1169 Quéguiner, B.: Pigments, elemental composition (C, N, P, Si) and stoichiometry of particulate
1170 matter, in the naturally iron fertilized region of Kerguelen in the Southern Ocean,
1171 Biogeosciences, 11, 5931–5955, 2014.

1172

1173 Laurenceau-Cornec, E. C., Trull, T. W., Davies, D. M., Bray, S. G., Doran, J., Planchon, F.,
1174 Carlotti, F., Jouandet, M. P., Cavagna, A. J., Waite, A. M., and Blain, S.: The relative importance
1175 of phytoplankton aggregates and zooplankton fecal pellets to carbon export: insights from free-
1176 drifting sediment trap deployments in naturally iron-fertilised waters near the Kerguelen plateau,
1177 Biogeosciences, 12, 1007–1027, 2015.

Le Quéré, C., Takahashi, T., Buitenhuis, E. T., Rödenbeck, C., and Sutherland, S. C.: Impact of climate change and variability on the global oceanic sink of CO2, Global Biogeochemical Cycles, 24(GB4007), doi:10.1029/2009GB003599, 2010.

Lenton, A., Tilbrook, B., Law, R. M., Bakker, D., Doney, S. C., Gruber, N., Ishii, M., Hoppema, M., Lovenduski, N. S., Matear, R. J., McNeil, B. I., Metzl, N., Mikaloff Fletcher, S. E., Monteiro, P. M. S., Rödenbeck, C., Sweeney, C., and Takahashi, T.: Sea-air CO_2 fluxes in the Southern Ocean for the period 1990–2009, Biogeosciences, 10, 4037–4054; doi:210.5194/bgd-5110-5285-5201, 2013.

Levitus, S.: Climatological atlas of the world ocean, NOAA Prof. Pap. 13, 173 pp., U.S. Govt. Printing Off., Washington, D. C., 1982.

Levy, M.: Mesoscale variability of phytoplankton and of new production: Impact of the large-scale nutrient distribution, Journal of Geophysical Research, 108(C11), 3358, doi:3310.1029/2002JC001577, 2003.

Maiti, K., Charette, M. A., Buesseler, K. O., and Kahru, M.: An inverse relationship between production and export efficiency in the Southern Ocean, Geophysical Research Letters, 40, 1557-1561, 2013.

Martin, J. H.: Glacial-interglacial CO_2 change: The iron hypothesis, Paleoceanography, 5, 1-13, 1990.

Martinez, E., Antoine, D., D'Ortenzio, F., and Gentili, B.: Climate-driven basin-scale decadal oscillations of oceanic phytoplankton, Science, 326, 1253-1256, 2009.

Matear, R., Hirst, A. C., and McNeil, B. I.: Changes in dissolved oxygen in the Southern Ocean with climate change, Geochemistry, Geophysics, Geosystems, 1(www.g-cubed.org), paper #2000GC000086, 2000.

Mongin, M., Molina, E., and Trull, T. W.: Seasonality and scale of the Kerguelen plateau phytoplankton bloom: A remote sensing and modeling analysis of the influence of natural iron fertilization in the Southern Ocean, Deep-Sea Research II, 55, 880-892, 10.1016/j.dsr2.2007.12.039, 2008.

Mongin, M., Abraham, E. R., and Trull, T. W.: Winter advection of iron can explain the summer phytoplankton bloom that extends 1000 km downstream of the Kerguelen Plateau in the Southern Ocean, Journal of Marine Research, 67, 225-237, 2009.

Moore, J. K., and Abbott, M. R.: Phytoplankton chlorophyll distributions and primary production in the Southern Ocean, *Journal of Geophysical Research*, *105*(C12), 28,709 –728,722, 2000.

Morel, A., and Maritorena, S.: Bio-optical properties of oceanic waters: A reappraisal, Journal of Geophysical Research, 106 (C4), 7163-7180, 2001.

Mosseri, J., Queguiner, B., Armand, L.K., and Cornet-Barthaux V.: Impact of iron on silicon utilization by diatoms in the Southern Ocean: A case study of Si/N cycle decoupling in a naturally iron-enriched area. Deep-Sea Research II, 55: 801-819, 2008.

Nicol, S., Pauly, T., Vindoff, N., Wright, S., Thiele, D., Hosie, G., Strutton, P., and Woehler, E.: Ocean circulation off East Antarctica affects ecosystem structure and sea-ice extent, Nature, 406, 504-507, 2000.

Nielsdóttir, M. C., Bibby, T. S., Moore, C. M., Hinz, D. J., Sanders, R., Whitehouse, M. J., Korb, R. E., and Achterberg, E. P.: Seasonal and spatial dynamics of iron availability in the Scotia Sea, Marine Chemistry. , 130-131, 62-72, 2012.

Oka, E., and Ando, K.: Stability of temperature and conductivity sensors of Argo profiling floats, Journal of oceanography, 60, 253-258, 2004.

Orsi, A. H., Whitworth, T. I., and Nowlin, W. D. J.: On the meridional extent and fronts of the Antarctic Circumpolar Current, Deep-Sea Research, 42, 641-673, 1995.

Park, Y.-H., Fuda, J.-L., Durand, I., and Naveira Garabato, A. C.: Internal tides and vertical mixing over the Kerguelen Plateau, Deep Sea Research Part II: Topical Studies in Oceanography, 55, 582-593, 2008a.

Park, Y.-H., Roquet, F., Fuda, J.-L., and Durand, I.: Large scale circulation over and around the Kerguelen Plateau, Deep Sea Research II, 55, 566-581, 2008b.

Park, Y.-H., Charriaud, E., Ruiz Pino, D., and Jeandel, C.: Seasonal and interannual variability of the mixed layer properties and steric height at station KERFIX, southwest of Kerguelen, Journal of Marine Systems, 17, 571–586, 1998.

Park, Y.-H., Durand, I., Kestenare, E., Rougier, G., Zhou, M., d'Ovidio, F., Cotté, C., and Lee, J.-H.: Polar Front around the Kerguelen Islands: An up-to-date determination and associated

circulation of surface/subsurface waters, Journal of Geophysical Research Oceans, 119, 6575–6592, doi:10.1002/2014JC010061, 2014a.

Park, Y.-H., Lee, J.-H., Durand, I., and Hong, C.-S.: Validation of the Thorpe scale-derived vertical diffusivities against microstructure measurements in the Kerguelen region, Biogeosciences, 11, 6927-6937, 2014b.

Parslow, J., Boyd, P., Rintoul, S. R., and Griffiths, F. B.: A persistent sub-surface chlorophyll maximum in the Polar Frontal Zone south of Australia: seasonal progression and implications for phytoplankton-light-nutrient interactions, Journal of Geophysical Research, 106, 31543-31557, 2001.

Planchon, F., Ballas, D., Cavagna, A.-J., Bowie, A., Davies, D., Trull, T., Laurenceau, E., van der Merwe, P., and Dehairs, F.: Carbon export in the naturally iron-fertilized Kerguelen area of the Southern Ocean based on the ^{234}Th approach, Biogeosciences Discuss., 11, submitted, 2014.

Pollard, R. T., I.Salter, Sanders, R. J., Lucas, M. I., Moore, C. M., Mills, R. A., Statham, P. J., Allen, J. T., Baker, A. R., Bakker, D. C. E., Charette, M. A., Fielding, S., Fones, G. R., French, M., Hickman, A. E., Holland, R. J., Hughes, J. A., Jickells, T. D., Lampitt, R. S., Morris, P. J., Nédélec, F. H., Nielsdóttir, M., Planquette, H., Popova, E. E., Poulton, A. J., Read, J. F., Seeyave, S., Smith, T., Stinchcombe, M., Taylor, S., Thomalla, S., Venables, H. J., Williamson, R., and Zubkov, M. V.: Southern Ocean deep-water carbon export enhanced by natural iron fertilization, Nature, 457, 577-580, doi:510.1038/nature07716, 2009.

Queguiner, B.: Iron fertilization and the structure of planktonic communities in high nutrient regions of the Southern Ocean, Deep Sea Research II, 90, 43-54, 2013.

Sackmann, B. S., Perry, M. J., and Eriksen, C. C.: Seaglider observations of variability in daytime fluorescence quenching of chlorophyll-a in Northeastern Pacific coastal waters, Biogeosciences Discussions, 5, 2839–2865, 2008.

Sallée, J.-B., Speer, K., Rintoul, S., and Wijffels, S.: Southern Ocean thermocline ventilation, Journal of Physical Oceanography, 40, 509-529, 2010.

Salter, I., Lampitt, R. S., Sanders, R., Poulton, A., Kemp, A. E. S., Boorman, B., Saw, K., and Pearce, R.: Estimating carbon, silica and diatom export from a naturally fertilised phytoplankton bloom in the Southern Ocean using PELAGRA: A novel drifting sediment trap, Deep Sea Research II, 54, 2233-2259, 2007.

Sanial, V., van Beek, P., Lansard, B., d'Ovidio, F., Kestenare, E., Souhaut, M., Zhou, M., and Blain, S.: Study of the phytoplankton plume dynamics off the Crozet Islands (Southern Ocean): A geochemical- physical coupled approach, Journal of Geophysical Research: Oceans, 119.4 2227-2237, 2014.

Sarmiento, J. L., Thiele, G., Key, R. M., and Moore, W. S.: Oxygen and nitrate new production and remineralization i the North Atlantic subtropical gyre, Journal of Geophysical Research: Oceans, 95, 18303-18315, 1990.

Sarmiento, J. L., and Le Quéré, C.: Oceanic carbon dioxide uptake in a model of century-scale global warming, Science, 274, 1346-1350, 1996.

Sarmiento, J. L., Gruber, N., Brzezinski, M. A., and Dunne, J. P.: High-latitude controls of thermocline nutrients and low latitude biological productivity, Nature, 427, 56-60, 2004.

Savoye, N., Dehairs, F., Elskens, M., Cardinal, D., Kopczynska, E. E., Trull, T. W., Wright, S., Baeyens, W., and Griffiths, F. B.: Regional variation of spring N-uptake and new production in the Southern Ocean, Geophysical Research Letters, 31, L03301, doi:03310.01029/02003GL018946, 2004.

Savoye, N., Trull, T. W., Jacquet, S. H. M., Navez, J., and Dehairs, F.: 234Th-based export fluxes during a natural iron fertilization experiment in the Southern Ocean (KEOPS), *Deep Sea Research II*, *55*(5-7), 841-855, 2008.

Schlitzer, R.: Carbon export fluxes in the Southern Ocean: results from inverse modeling and comparison with satellite-based estimates, Deep-Sea Research II, 49, 1623-1644, 2002.

Shadwick, E. H., Tilbrook, B., Cassar, N., Trull, T. W., and Rintoul, S. R.: Summertime physical and biological controls on O_2 and CO_2 in the Australian Sector of the Southern Ocean, Journal of Marine System, doi: 10.1016/j.jmarsys.2013.12.008, 2014.

Shadwick, E. H., Trull, T. W., Tilbrook, B., Sutton, A., Schulz, E., and Sabine, C. L.: Seasonality of biological and physical controls on surface ocean CO_2 from hourly observations at the Southern Ocean Time Series site south of Australia, Global Biogeochemical Cycles, 29, 223–238, doi: 10.1002/2014GB004906, 2015.

Sigman, D. M., and Boyle, E. A.: Glacial/Interglacial variations in atmospheric carbon dioxide, Nature, 407, 859-869, 2000.

Sokolov, S., and Rintoul, S. R.: Circumpolar structure and distribution of the Antarctic Circumpolar Current fronts: 1. Mean circumpolar paths, Journal of geophysical research, 114, C11018, 2009.

Sokolov, S., and Rintoul, S. R.: On the relationship between fronts of the Antarctic Circumpolar Current and surface chlorophyll concentrations in the Southern Ocean, J. Geophys. Res. – Oceans, *112*(C07030), doi: 10.1029/2006JC004072, 2007.

Spitzer, W. S., and Jenkins, W. J.: Rates of vertical mixing, gas exchange and new production: Estimates from seasonal gas cycles in the upper ocean near Bermuda, Journal of Marine Research, 47, 169-196, 1989.

Stramski, D., Reynolds, R. A., Babin, M., Kaczmarek, S., Lewis, M. R., Röttgers, R., Sciandra, A., Stramska, M., Twardowski, M. S., Franz, B. A., and Claustre, H.: Relationships between the surface concentration of particulate organic carbon and optical properties in the eastern South Pacific and eastern Atlantic Oceans, Biogeosciences, 5, 171–201, 2008.

Suggett, D. J., Prášil, O., and Borowitzka, M. A.: *Chlorophyll a fluorescence in aquatic sciences: methods and applications*, Springer, 2011.

Sullivan, J. M., Twardowski, M. S., Zaneveld, R. J. V., and Moore, C. C.: Measuring optical backscattering in water, in Light Scattering Reviews 7: Radiative Transfer and Optical Properties of Atmosphere and Underlying Surface, A. Kokhanovsky, ed. (Springer Praxis Books, 2013), pp. 189–224.

Sverdrup, H. U.: On the conditions for the vernal blooming of phytoplankton, *Journal du Conseil Internationale Permanente pour l'Exploration de la Mer*, *18*, 287-295, 1953.

Swart, S., Thomalla, S., and Monteiro, P.: The seasonal cycle of mixed layer dynamics and phytoplankton biomass in the Sub-Antarctic Zone: A high-resolution glider experiment, *Journal of Marine Systems*, 2014.

Taylor, J. R., and Ferrari, R.: Shutdown of turbulent convection as a new criterion for the onset of spring phytoplankton blooms, *Limnology and Oceanography*, *56*(6), 2293–2307, 2011.

Thomalla, S. J., Fauchereau, N., Swart, S., and Monteiro, P. M. S.: Regional scale characteristics of the seasonal cycle of chlorophyll in the Southern Ocean, Biogeosciences, 8(10), 2849-2866, doi:10.5194/bg-8-2849-2011, 2011.

Trull, T. W., Davies, D., and Casciotti, K.: Insights into nutrient assimilation and export in naturally iron-fertilized waters of the Southern Ocean from nitrogen, carbon and oxygen isotopes, Deep-Sea Research Part Ii-Topical Studies in Oceanography, 55, 820-840, 10.1016/j.dsr2.2007.12.035, 2008.

Trull, T. W., Davies, D. M., Dehairs, F., Cavagna, A. J., Lasbleiz, M., Laurenceau, E. C., d'Ovidio, F., Planchon, F., Leblanc, K., Quéguiner, B., and Blain, S.: Chemometric perspectives on plankton community responses to natural iron fertilization over and downstream of the Kerguelen Plateau in the Southern Ocean, Biogeosciences, 12, 1029–1056, 2015.

Trull, T. W., Bray, S. G., Manganini, S. J., Honjo, S., and François, R.: Moored sediment trap measurements of carbon export in the Subantarctic and Polar Frontal Zones of the Southern Ocean, south of Australia, Journal of Geophysical Research, 106, 31489-31510, 2001.

Watson, A. J., Bakker, D. C. E., Ridgwell, A. J., Boyd, P. W., and Law, C. S.: Effect of iron supply on Southern Ocean CO2 uptake and implications for glacial for atmospheric CO_2, Nature, 407, 730-733, 2000.

Weeding, B., and Trull, T. W.: Hourly oxygen and total gas tension measurements at the Southern Ocean Time Series site reveal winter ventilation and spring net community production, Journal of Geophysical Research - Oceans, 119, 348-358, doi:310.1002/2013JC009302, 002014, 2014.

Xing, X., Claustre, H., Blain, S., d'Ortenzio, F., Antoine, D., Ras, J., and Guinet, C.: Quenching correction for in vivo chlorophyll fluorescence acquired by autonomous platforms: A case study with instrumented elephant seals in the Kerguelen region (Southern Ocean), Limnology and Oceanography: Methods, 10, 483–495, 2012.

Zhang, X., Hu, L., and He, M.-X.: Scattering by pure seawater: effect of salinity, Opt.Express, 17, 5698–5710, 2009.

Table 1. Bio-profiler deployments

#	Hull#*	WMO#**	UTC Date	Lat. (° N)	Long. (° E)	Campaign	Last profile (UTC Date)
1	5122	1901329	29 Oct 2011	-48.5	72.2	KEOPS2	22 Apr 2012
2	6684	5904882	26 Jan 2014	-49.9	76.2	MYCTO	14 Apr 2014
3	6682	1901338	28 Jan 2014	-48.4	71.5	MYCTO	14 Apr 2014
4	6683	1901339	4 Feb 2014	-48.6	74.0	MYCTO	14 Apr 2014

* Hull#: serial number for the bio-profiler body

** WMO#: World Meteorological Organization identification number for the bio-profiler data stream

Table 2. Drift assessment of the bio-profilers over their life time within the [250-300] m and [950-1000] m depth layers

Chlorophyll concentration *drift within the* ***[250-300]*** *m depth layer*

#	Mean slope ($\mu g\ L^{-1}$ $profile^{-1}$)	Mean absolute drift[a] ($\mu g\ L^{-1}$)	Mean drift relative to the mean surface Chl-a concentration[b]
1[c]	8.4050 E-5	0.0252	+1 %
2	-1.7832 E-4	-0.0531	-5 %
3	-2.8722 E-4	-0.0798	-6 %
4	-1.1976 E-4	-0.0304	-3 %

Chlorophyll concentration *drift within the* ***[950-1000]*** *m depth layer*

#	Mean slope ($\mu g\ L^{-1}$ $profile^{-1}$)	Mean absolute drift[a] ($\mu g\ L^{-1}$)	Mean drift relative to the mean surface Chl-a concentration[b]
1	–	–	–
2	-2.1917 E-6	-0.0007	< -1 %
3	-9.0120 E-5	-0.0251	-2 %
4	1.2438 E-5	0.0032	< +1 %

Particulate backscattering *drift within the* ***[250-300]*** *m depth layer*

#	Mean slope (m^{-1})	Mean absolute drift[a] (m^{-1})	Mean drift relative to the mean surface b_{bp}[d]
1[c]	1.1625 E-6	3.4876 E-04	+11 %
2	-1.1613 E-6	-3.4608 E-04	-19 %
3	-1.9682 E-7	-5.4716 E-05	-2 %
4	-6.7301 E-7	-1.7094 E-04	-10 %

Particulate backscattering *drift within the* ***[950-1000]*** *m depth layer*

#	Mean slope (m^{-1})	Mean absolute drift[a] (m^{-1})	Mean drift relative to the mean surface b_{bp}[d]
1	–	–	–
2	-2.2931 E-7	-6.8335 E-05	-4 %
3	-4.4734 E-7	-1.2436 E-04	-6 %
4	-2.0227 E-7	-5.1378 E-05	-3 %

[a] = mean slope * nb of profiles

[b] = mean slope * nb of profiles / mean chlorophyll concentration

[c] Calculated between profiles #1 and profile #300, and excluding the deep biomass production profiles (range #[100-171])

[d] = mean slope * nb of profiles / mean particulate backscattering

1452 Table 3. Fluorescence quenching corrections and subsurface chlorophyll maxima statistics

1453

Individual bio-profiler statistics	**#1**	**#2**	**#3**	**#4**
Fluorescence profiles collected	384	298	278	254
Fluorescence profiles usable	300	298	277	254
Night time profiles	129	143	133	119
Day time profiles	171	155	144	135
Night time profiles with subsurface maxima[a] **total**/within the ML/below the ML (% of night time profiles)	**17**/5/12/ (13/4/9)%	**3**/1/2 (2/1/1)%	**24**/9/15 (18/7/11)%	**25**/14/11 (21/12/9)%
Day time profiles with subsurface maxima[a] before correction **total**/within the ML/below the ML (% of daytime profiles)	**142**/62/80 (83/36/47)%	**93**/55/38 (60/35/25)%	**105**/48/57 (73/33/40)%	**95**/40/55 (70/30/40)%
Quenching corrected profiles (and among them, number of corrected profiles which still exhibit low surface values[c])	170 (22)	155 (6)	139 (12)	127 (18)
Day time profiles with subsurface maxima[a] after correction **total**/within the ML/below the ML (% of corrected day profiles)	**40**/0/40 (24/0/24)%	**10**/1/9 (6/0/6)%	**32**/3/29 (23/2/21)%	**40**/9/31 (31/7/24)%
Total night and corrected day profiles with **moderate** subsurface maxima[a] **total**/within the ML/below the ML (% of night and corrected day profiles)	**57**/5/52 (19/2/17)%	**13**/2/11 (4/1/3)%	**56**/12/44 (20/4/16)%	**65**/23/42 (26/9/17)%
Total night and corrected day profiles with **large** subsurface maxima[b] **total**/within the ML/below the ML (% of night and corrected day profiles)	**32**/1/31 (10/0/10)%	**6**/0/6 (2/0/2)%	**36**/5/31 (13/2/11)%	**45**/15/30 (18/6/12)%

1454 [a] Subsurface values exceeding surface values by more than 60%

1455 [b] Subsurface values exceeding surface values by more than 100%

1456 [c] For some corrected profiles, a large decrease of the chlorophyll concentration still occurred in the
1457 surface layer. These profiles were flagged in Figures 2b (squares), 4 (squares) and 5 (red circles).
1458 See the method section and the caption of Figure 2b for more details.

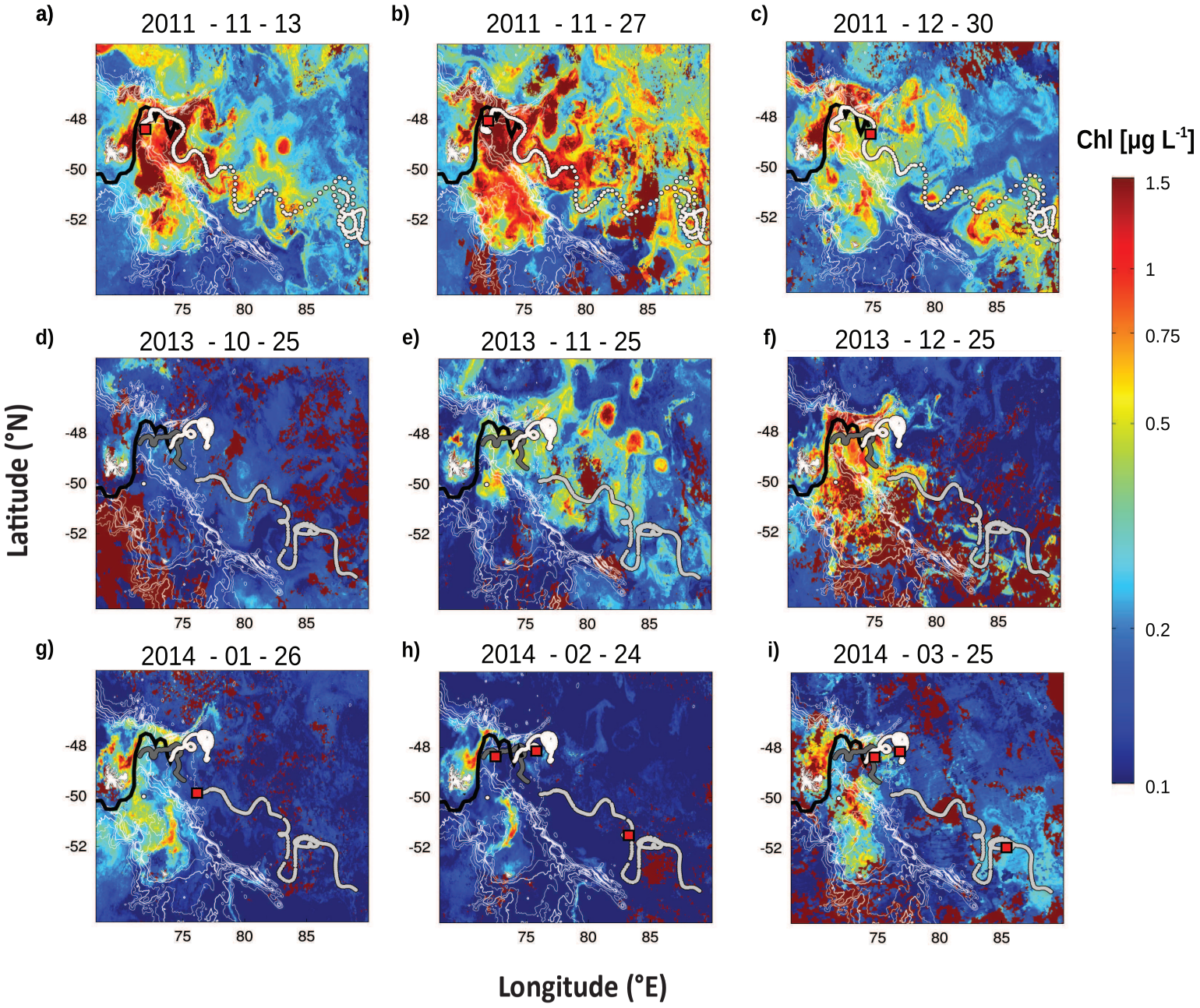
a)
2011 - 11 - 13
b)
2011 - 11 - 27
c)
2011 - 12 - 30
d)
2013 - 10 - 25
e)
2013 - 11 - 25
f)
2013 - 12 - 25
g)
2014 - 01 - 26
h)
2014 - 02 - 24
i)
2014 - 03 - 25
-48
-50
-52
75
80
85
Latitude (°N)
Longitude (°E)
Chl [µg L-1]
1.5
1
0.75
0.5
0.2
0.1

a) Drifting assessment

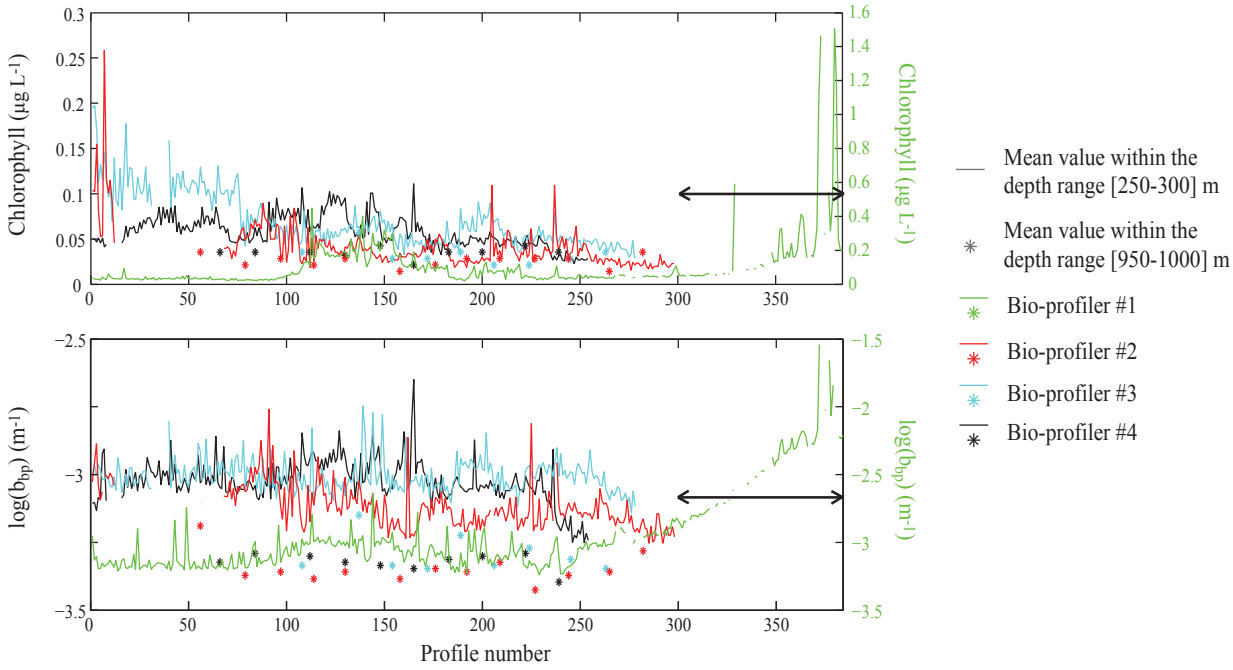

b) Quenching assessment

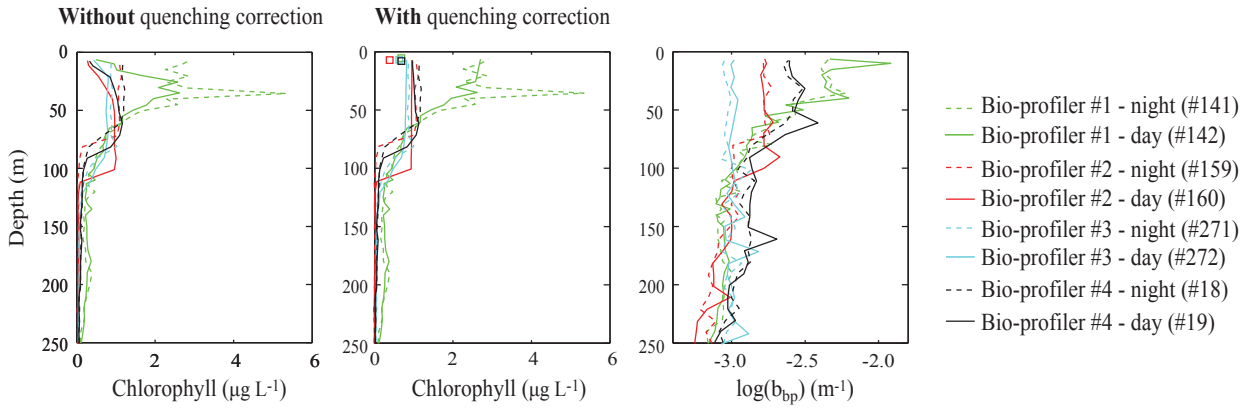

c) Comparison to KEOPS2 shipboard observations

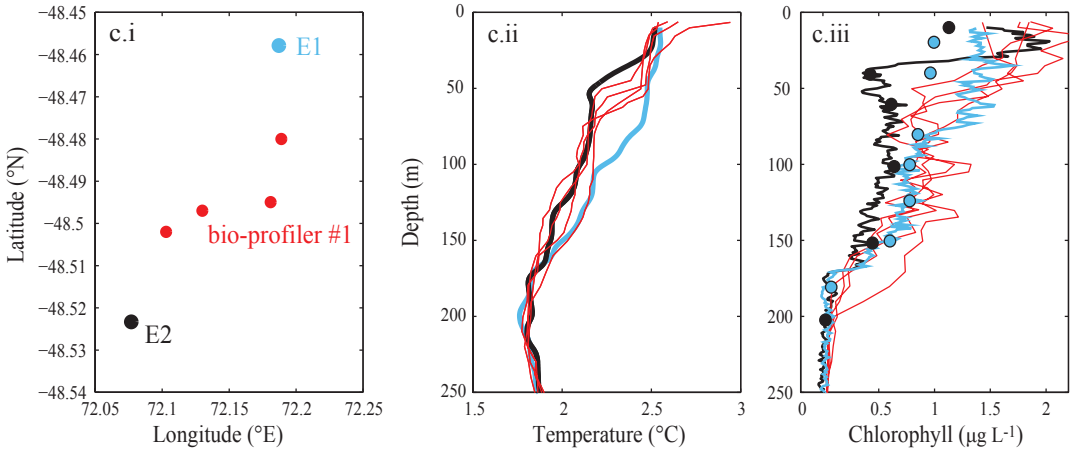

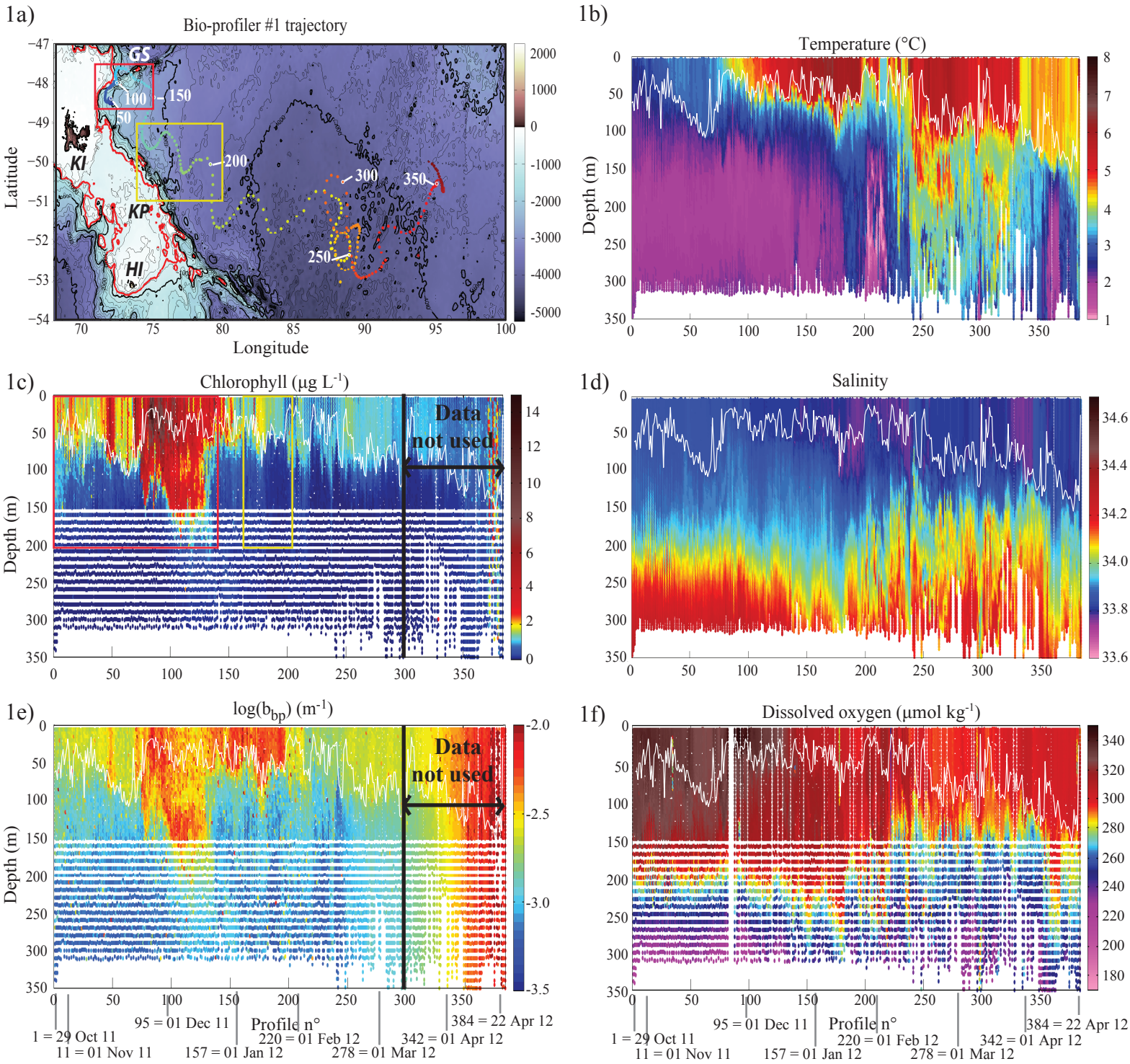
1a)
Bio-profiler #1 trajectory
GS
KI
KP
HI
50
100
150
200
250
300
350
Latitude
Longitude
1b)
Temperature (°C)
Depth (m)
1c)
Chlorophyll (µg L-1)
Data not used
Depth (m)
1d)
Salinity
1e)
log(bbp) (m-1)
Data not used
Depth (m)
1f)
Dissolved oxygen (µmol kg-1)
95 = 01 Dec 11
Profile n°
384 = 22 Apr 12
1 = 29 Oct 11
11 = 01 Nov 11
157 = 01 Jan 12
220 = 01 Feb 12
278 = 01 Mar 12
342 = 01 Apr 12

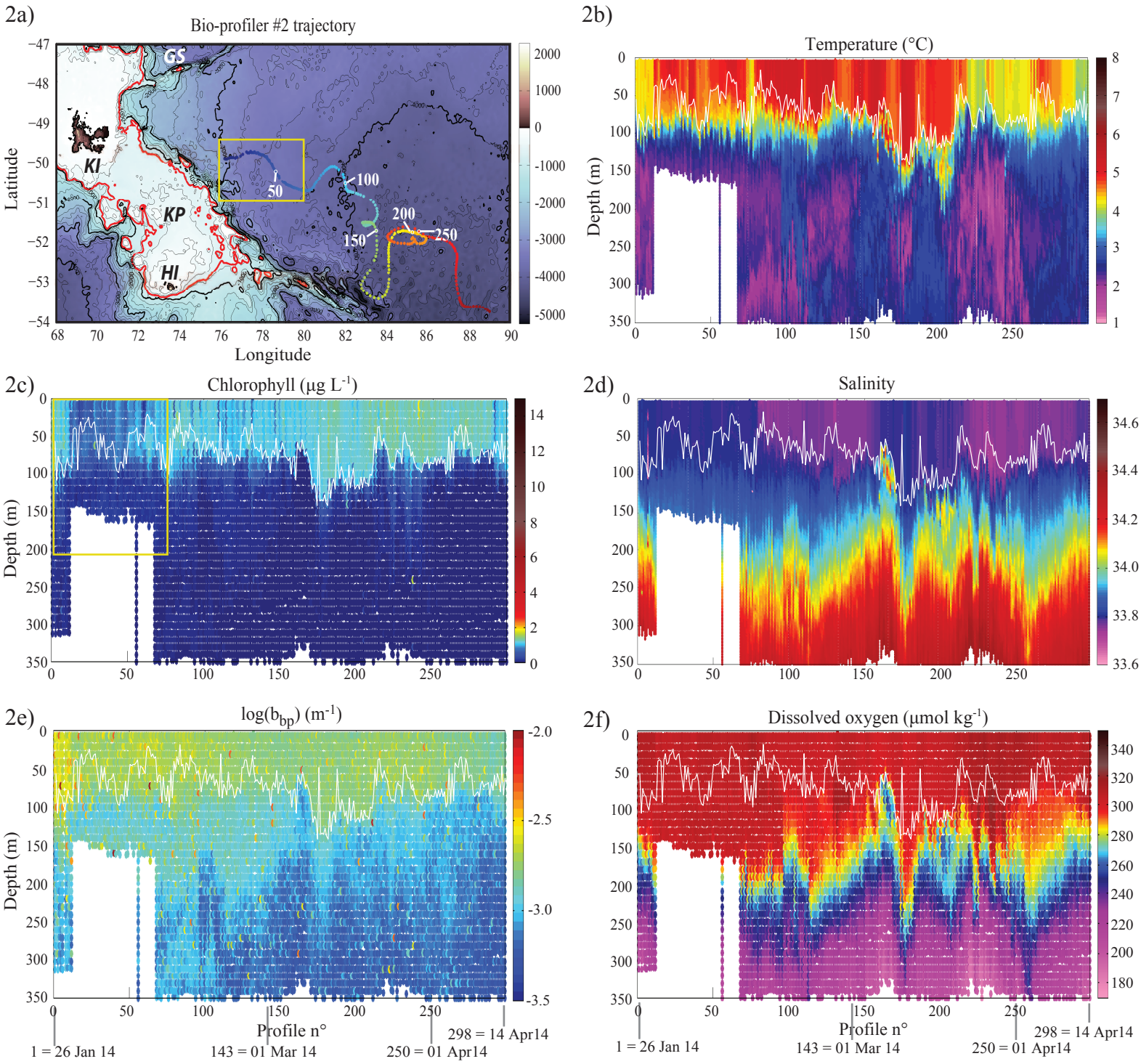
2a)
Bio-profiler #2 trajectory
GS
KI
KP
HI
1
50
100
150
200
250
Latitude
Longitude
2b)
Temperature (°C)
Depth (m)
2c)
Chlorophyll (µg L-1)
Depth (m)
2d)
Salinity
2e)
log(bbp) (m-1)
Depth (m)
Profile n°
1 = 26 Jan 14
143 = 01 Mar 14
250 = 01 Apr14
298 = 14 Apr14
2f)
Dissolved oxygen (µmol kg-1)
Profile n°
1 = 26 Jan 14
143 = 01 Mar 14
250 = 01 Apr14
298 = 14 Apr14

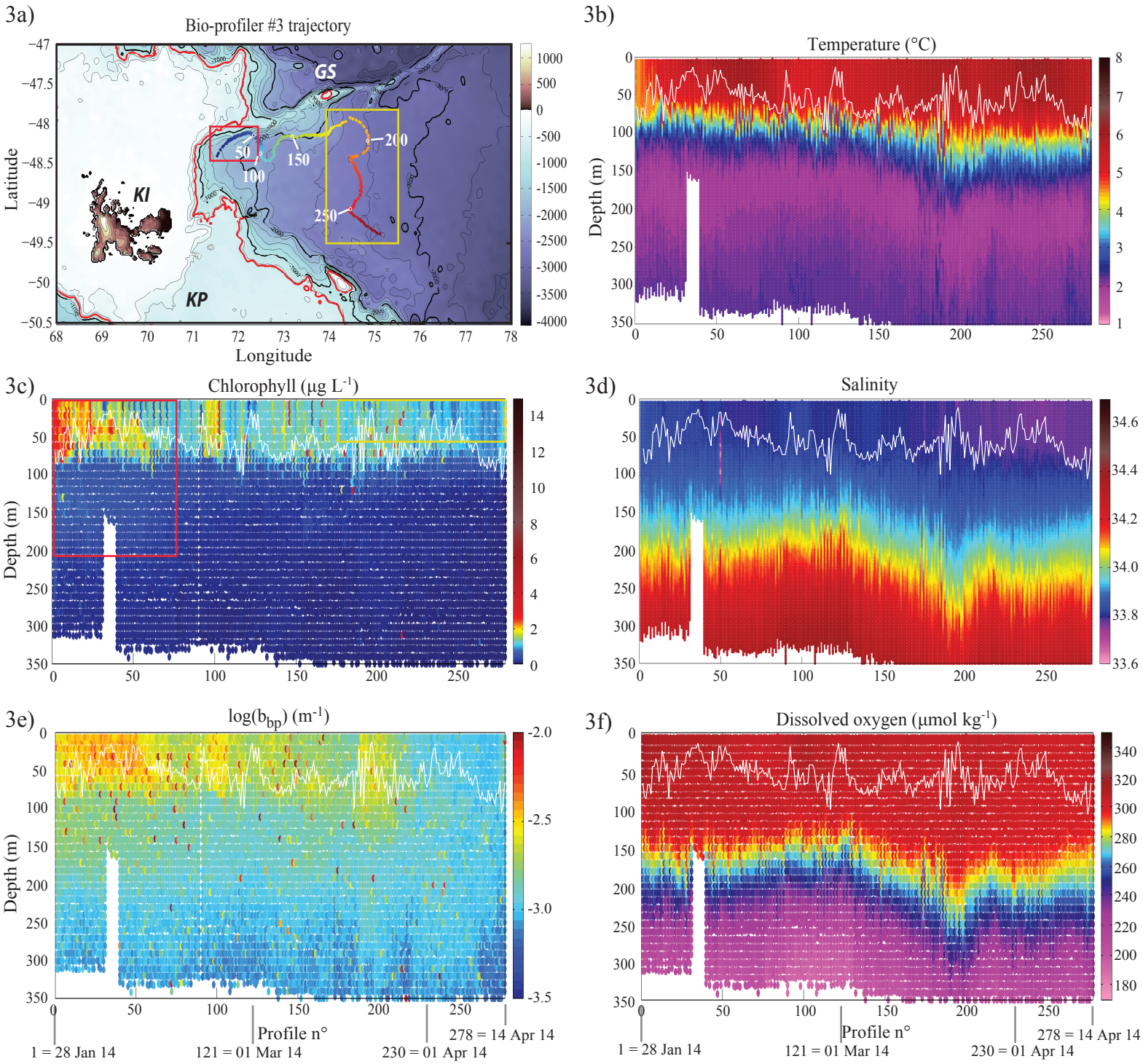
3a)
Bio-profiler #3 trajectory
GS
KI
KP
50
100
150
200
250
Latitude
Longitude
3b)
Temperature (°C)
Depth (m)
3c)
Chlorophyll (µg L-1)
Depth (m)
3d)
Salinity
3e)
log(bbp) (m-1)
Depth (m)
3f)
Dissolved oxygen (µmol kg-1)
Profile n°
1 = 28 Jan 14
121 = 01 Mar 14
230 = 01 Apr 14
278 = 14 Apr 14

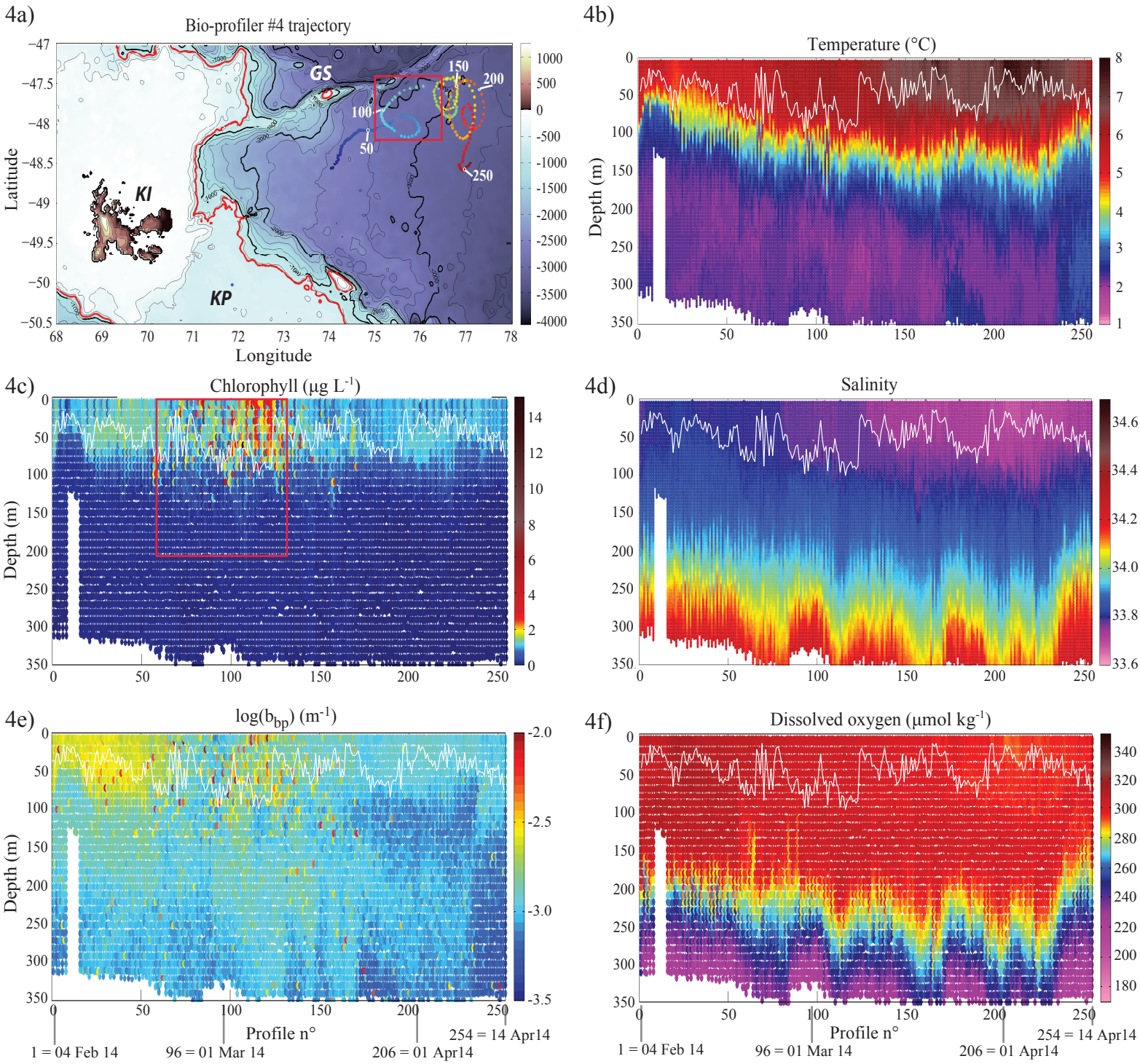
4a)
Bio-profiler #4 trajectory
GS
KI
KP
150
200
100
50
250
Latitude
Longitude
4b)
Temperature (°C)
Depth (m)
4c)
Chlorophyll (µg L-1)
Depth (m)
4d)
Salinity
4e)
log(bbp) (m-1)
Depth (m)
Profile n°
1 = 04 Feb 14
96 = 01 Mar 14
206 = 01 Apr14
254 = 14 Apr14
4f)
Dissolved oxygen (µmol kg-1)
Profile n°
1 = 04 Feb 14
96 = 01 Mar 14
206 = 01 Apr14
254 = 14 Apr14

Areas where subsurface chlorophyll maximum exceeds the surface content of more than 60%

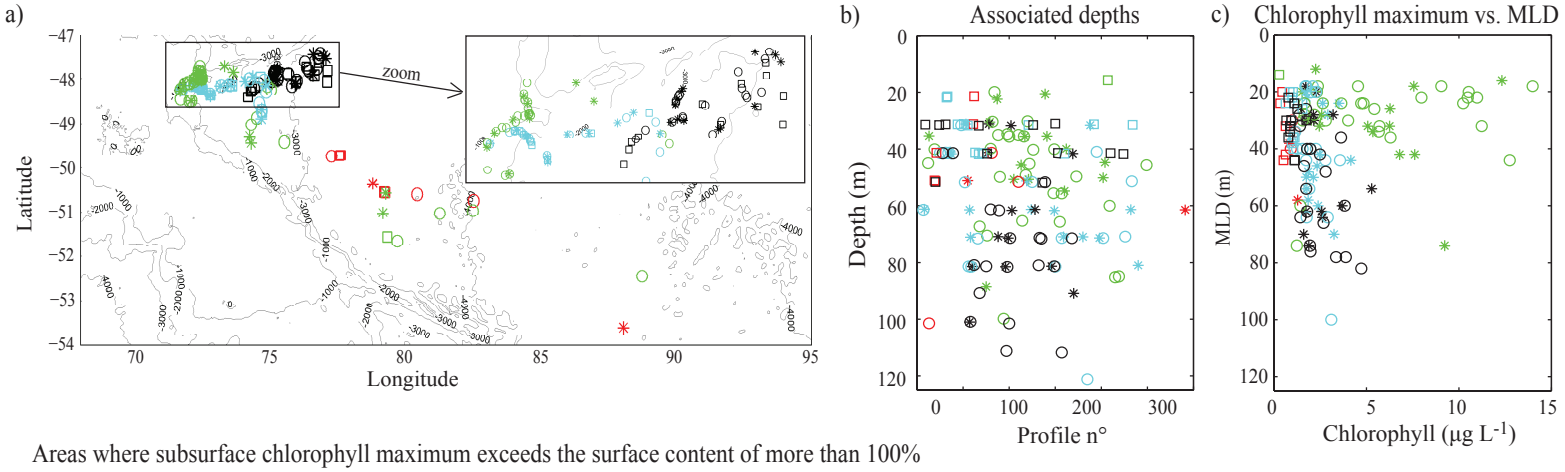

Areas where subsurface chlorophyll maximum exceeds the surface content of more than 100%

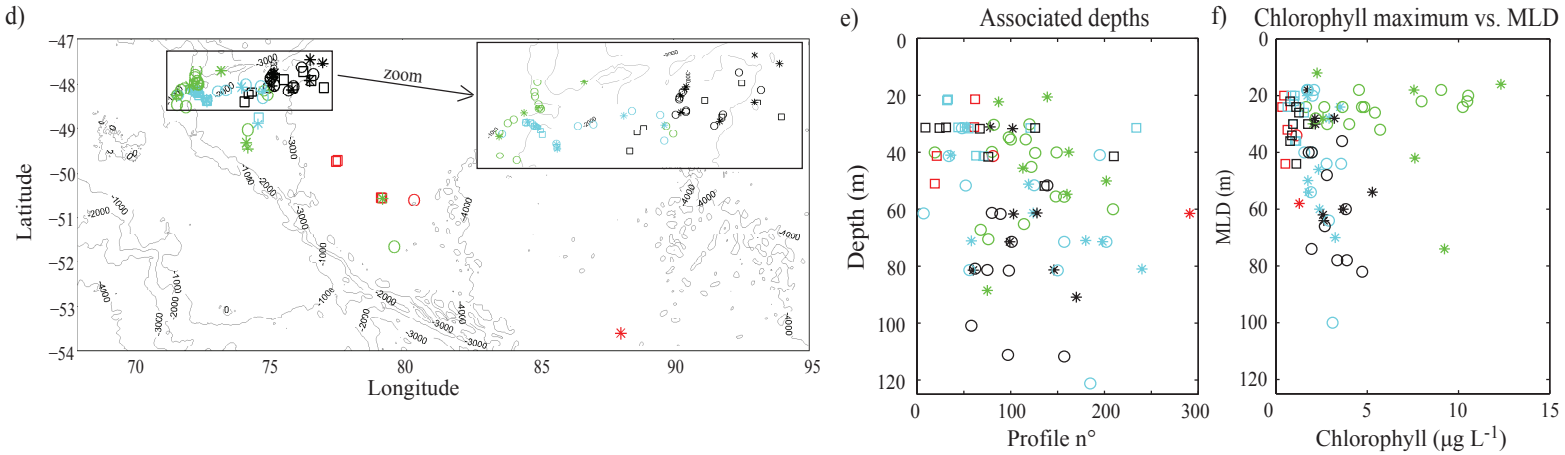

Bio-profiler #1 Bio-profiler #2 Bio-profiler #3 Bio-profiler #4

✳ Night profiles ○ Corrected day profiles □ Corrected day profiles which still exibit, in the surface layer, a large concentration decrease toward low surface values

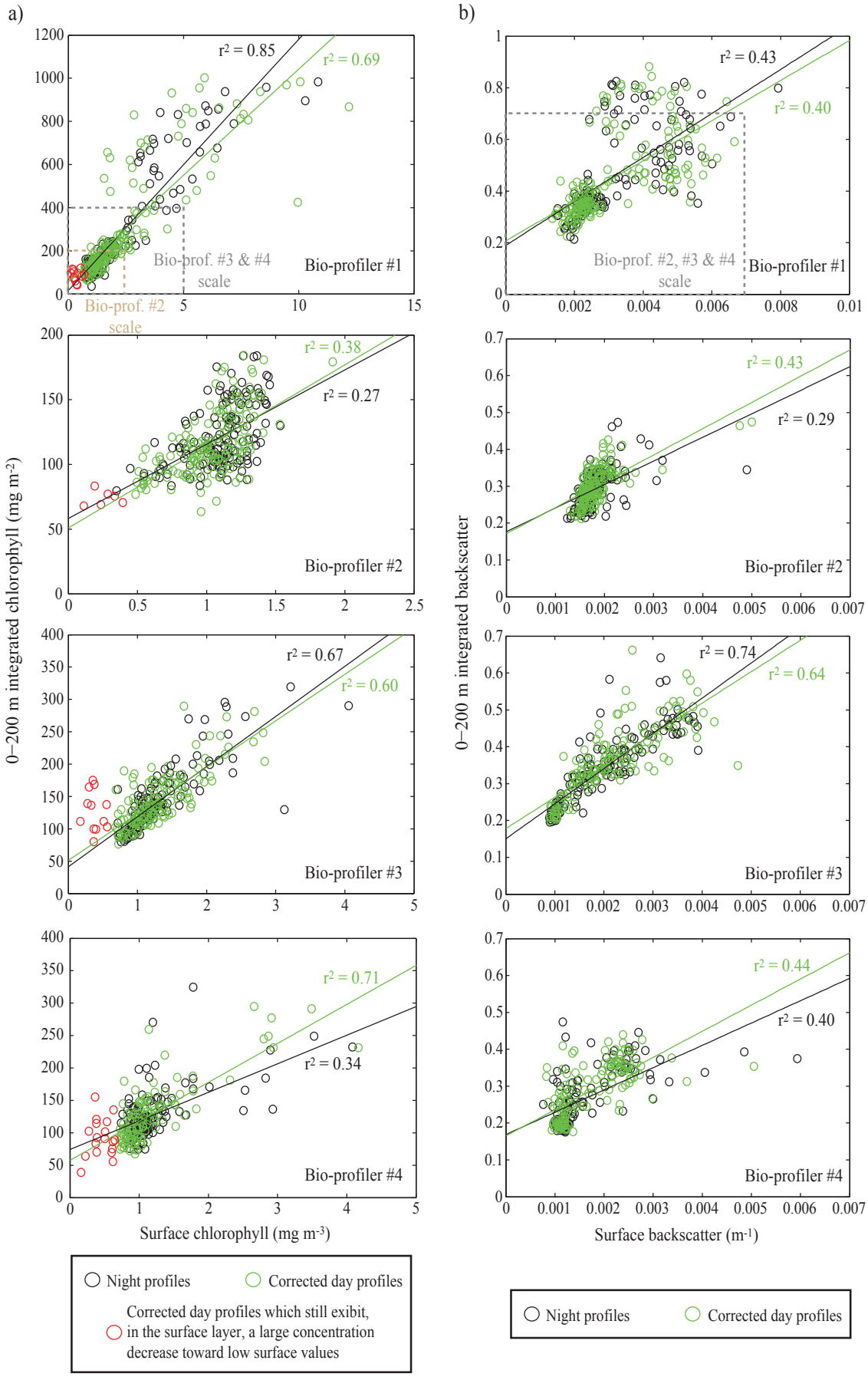
a)
b)
r² = 0.85
r² = 0.69
Bio-prof. #3 & #4 scale
Bio-prof. #2 scale
Bio-profiler #1
r² = 0.43
r² = 0.40
Bio-prof. #2, #3 & #4 scale
Bio-profiler #1
r² = 0.38
r² = 0.27
Bio-profiler #2
r² = 0.43
r² = 0.29
Bio-profiler #2
r² = 0.67
r² = 0.60
Bio-profiler #3
r² = 0.74
r² = 0.64
Bio-profiler #3
r² = 0.71
r² = 0.34
Bio-profiler #4
r² = 0.44
r² = 0.40
Bio-profiler #4
0–200 m integrated chlorophyll (mg m-2)
0–200 m integrated backscatter
Surface chlorophyll (mg m-3)
Surface backscatter (m-1)
Night profiles
Corrected day profiles
Corrected day profiles which still exibit, in the surface layer, a large concentration decrease toward low surface values
Night profiles
Corrected day profiles

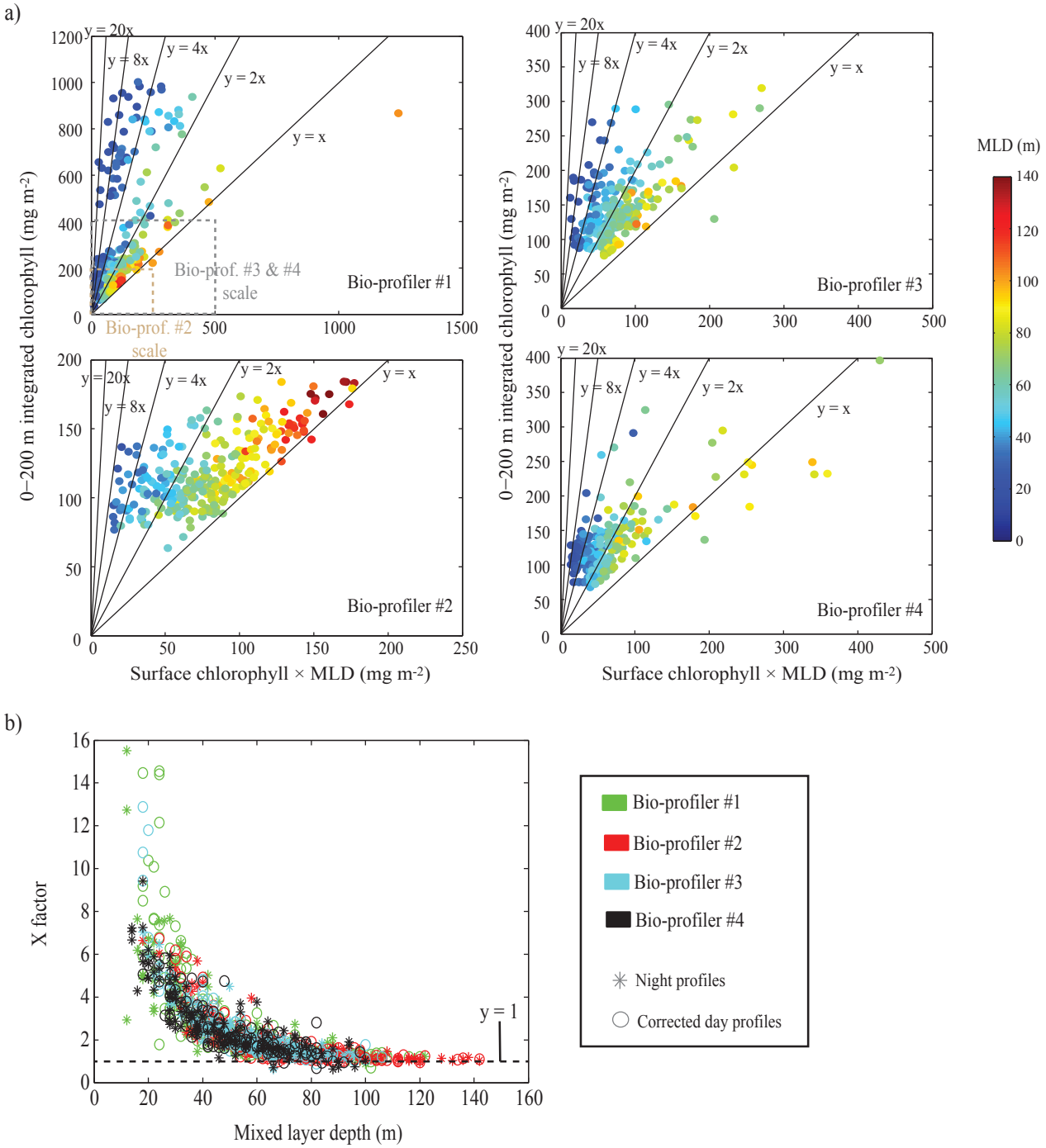
a)
y = 20x
y = 8x
y = 4x
y = 2x
y = x
Bio-prof. #3 & #4 scale
Bio-prof. #2 scale
Bio-profiler #1
Bio-profiler #2
Bio-profiler #3
Bio-profiler #4
0−200 m integrated chlorophyll (mg m-2)
Surface chlorophyll × MLD (mg m-2)
MLD (m)
b)
X factor
y = 1
Mixed layer depth (m)
Bio-profiler #1
Bio-profiler #2
Bio-profiler #3
Bio-profiler #4
Night profiles
Corrected day profiles

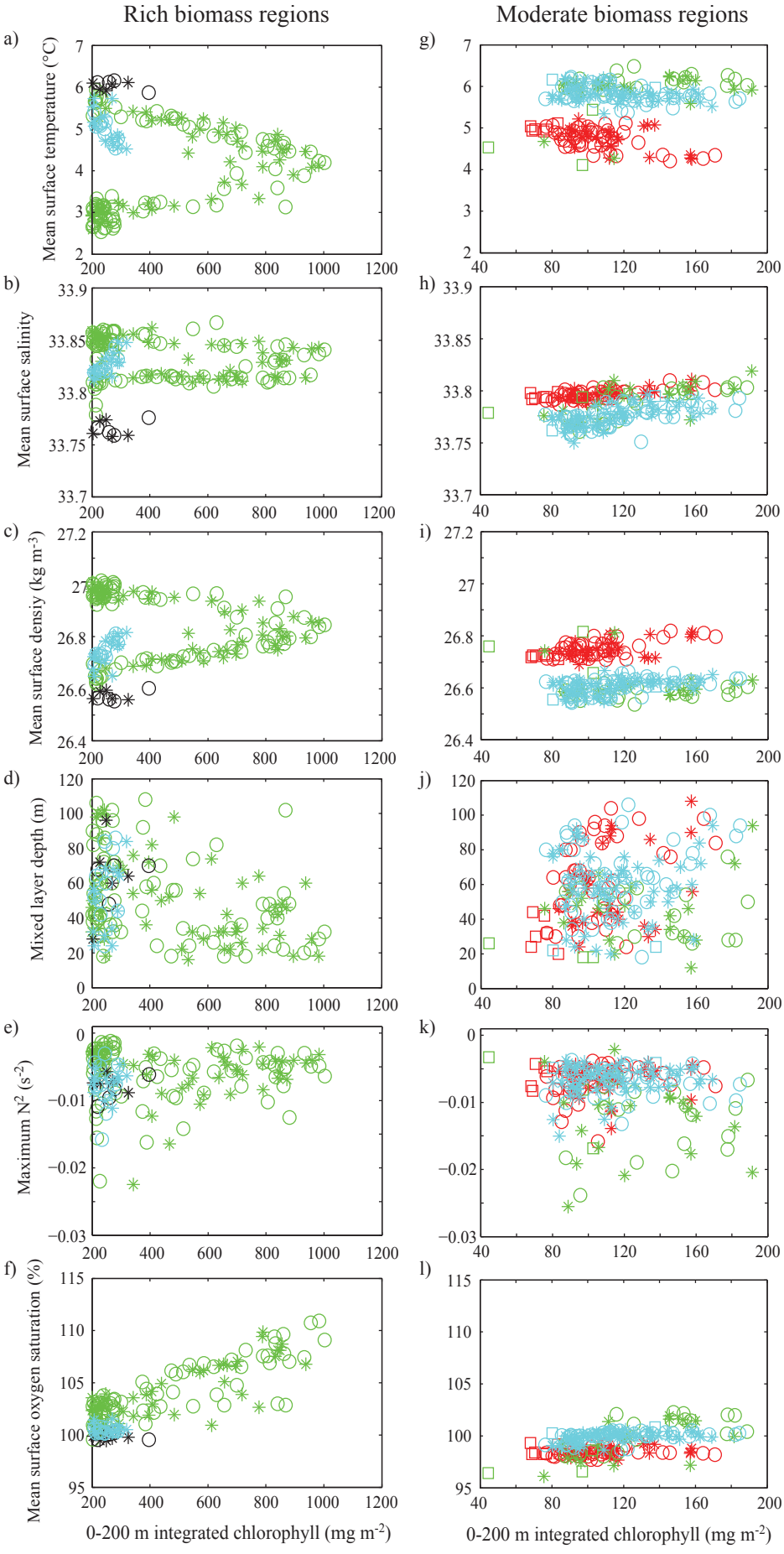
Rich biomass regions
Moderate biomass regions
a)
g)
b)
h)
c)
i)
d)
j)
e)
k)
f)
l)
Mean surface temperature (°C)
Mean surface salinity
Mean surface densiy (kg m-3)
Mixed layer depth (m)
Maximum N2 (s-2)
Mean surface oxygen saturation (%)
0-200 m integrated chlorophyll (mg m-2)
0-200 m integrated chlorophyll (mg m-2)
Bio-profiler #1
Bio-profiler #2
Bio-profiler #3
Bio-profiler #4
Night profiles
Corrected day profiles
Corrected day profiles which still exibit, in the surface layer, a large concentration decrease toward low surface values

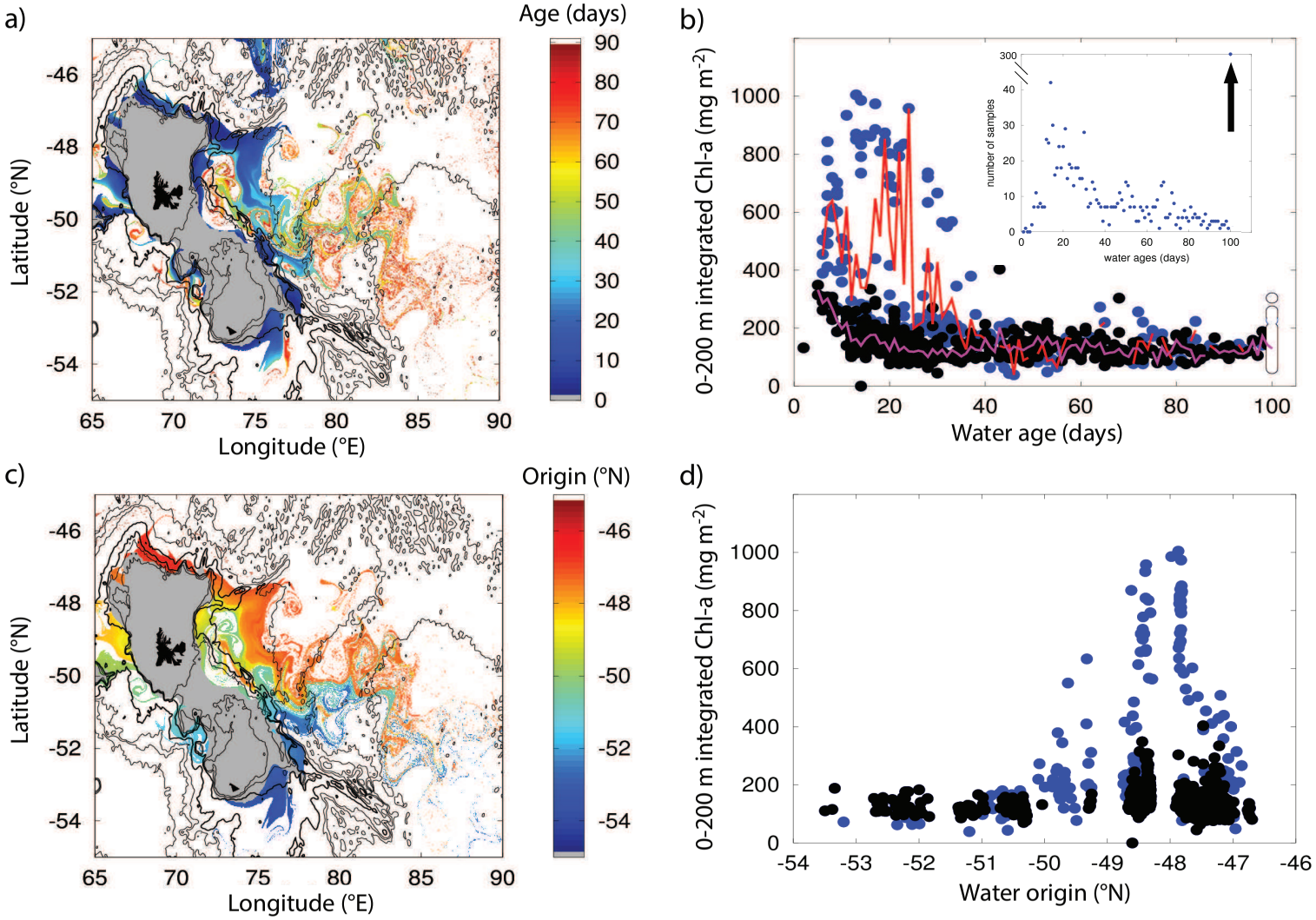
a)
Age (days)
90
80
70
60
50
40
30
20
10
0
-46
-48
-50
-52
-54
65
70
75
80
85
90
Latitude (°N)
Longitude (°E)
b)
0-200 m integrated Chl-a (mg m-2)
1000
800
600
400
200
0
0
20
40
60
80
100
Water age (days)
number of samples
300
40
30
20
10
0
0
20
40
60
80
100
water ages (days)
c)
Origin (°N)
-46
-48
-50
-52
-54
65
70
75
80
85
90
Latitude (°N)
Longitude (°E)
d)
0-200 m integrated Chl-a (mg m-2)
1000
800
600
400
200
0
-54
-53
-52
-51
-50
-49
-48
-47
-46
Water origin (°N)

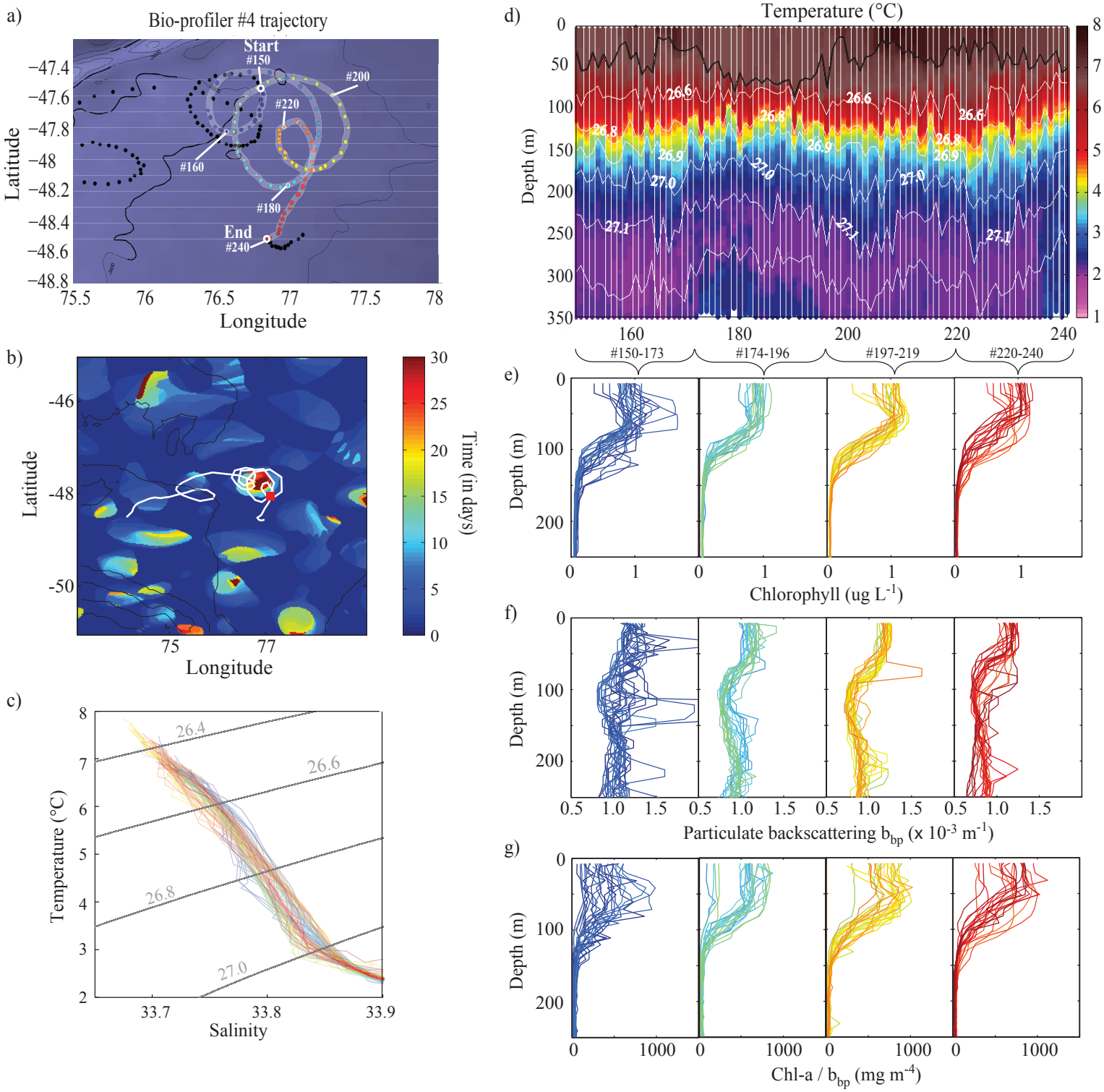
a)
Bio-profiler #4 trajectory
Start
#150
#200
#220
#160
#180
End
#240
Latitude
Longitude
b)
Latitude
Longitude
Time (in days)
c)
Temperature (°C)
Salinity
26.4
26.6
26.8
27.0
d)
Temperature (°C)
Depth (m)
#150-173
#174-196
#197-219
#220-240
e)
Depth (m)
Chlorophyll (ug L-1)
f)
Depth (m)
Particulate backscattering bbp (x 10-3 m-1)
g)
Depth (m)
Chl-a / bbp (mg m-4)

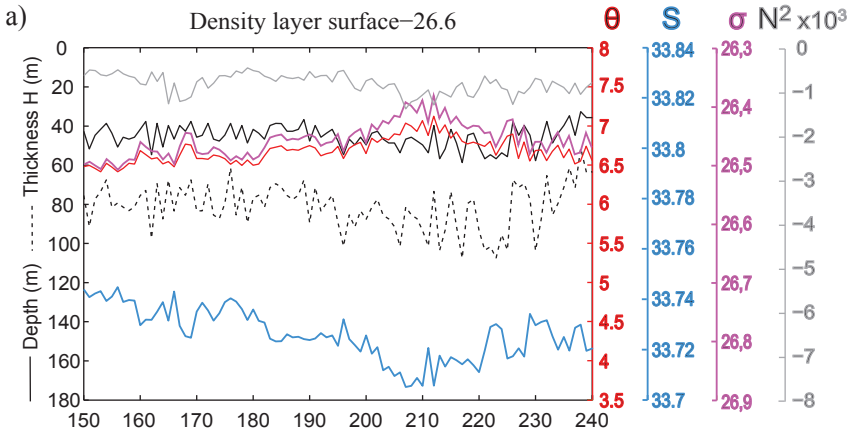
a)
Density layer surface−26.6
θ
S
σ
N² x10³
Thickness H (m)
Depth (m)

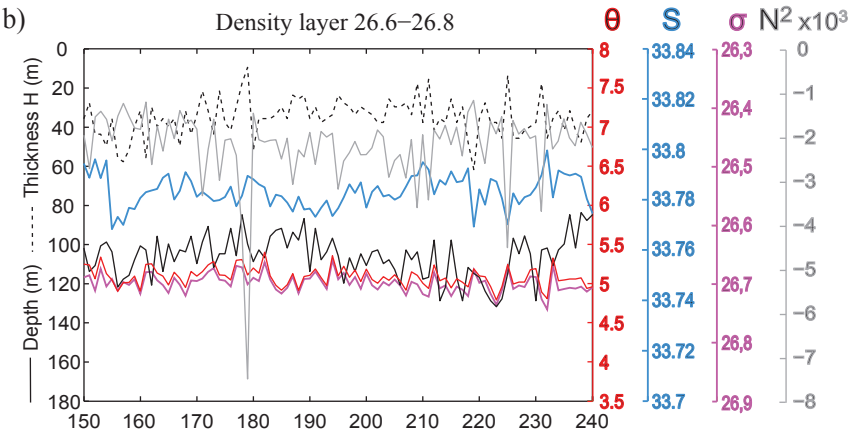
b)
Density layer 26.6−26.8
θ
S
σ
N² x10³
Thickness H (m)
Depth (m)

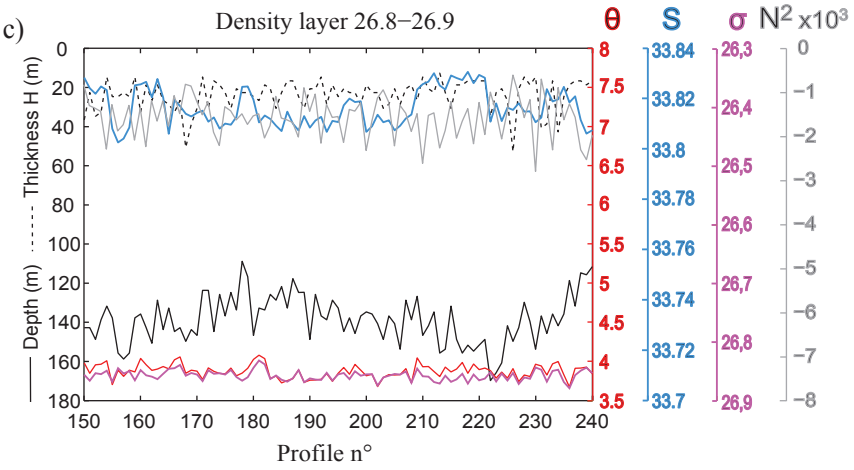
c)
Density layer 26.8−26.9
θ
S
σ
N² x10³
Thickness H (m)
Depth (m)
Profile n°

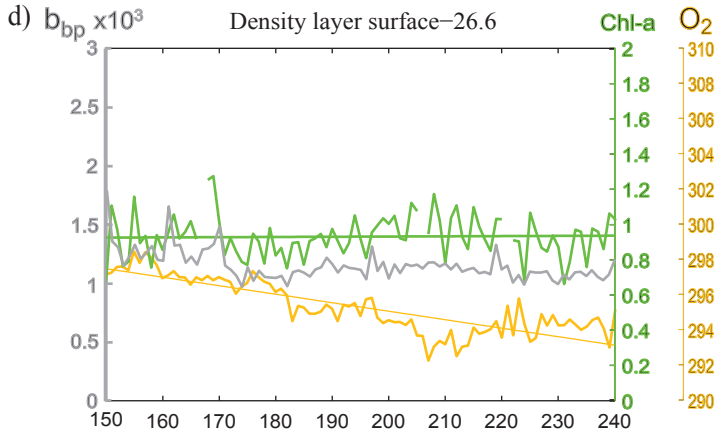
d)
b_bp x10³
Density layer surface−26.6
Chl-a
O₂

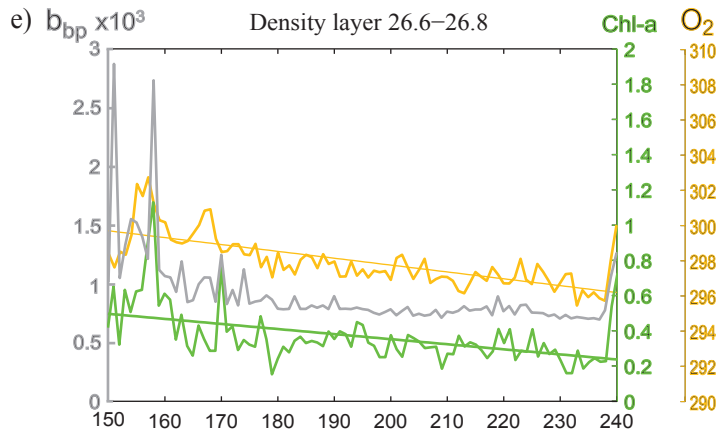
e)
b_bp x10³
Density layer 26.6−26.8
Chl-a
O₂

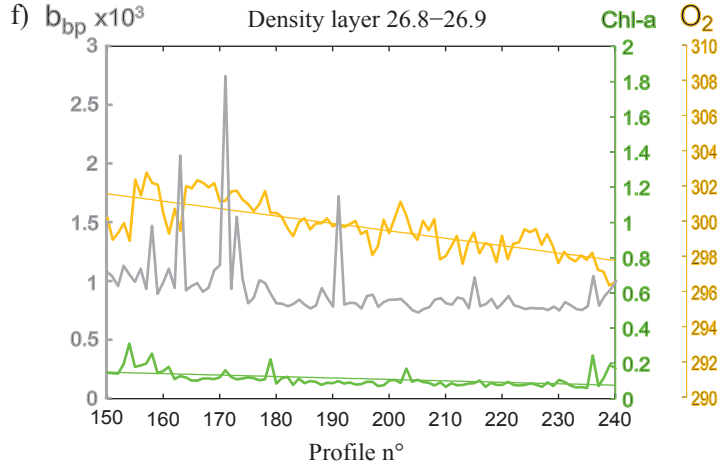
f)
b_bp x10³
Density layer 26.8−26.9
Chl-a
O₂
Profile n°